Acta Geodyn. Geomater., Vol. 22, No. 2 (218), 151–182, 2025
DOI: 10.13168/AGG.2025.0011

journal homepage: https://www.irsm.cas.cz/acta

ORIGINAL PAPER

GRAVITY STRIKE ANGLES TO STUDY VARIOUS GEOLOGICAL FEATURES

Jaroslav KLOKOČNÍK [1] *, Václav CÍLEK [2], Jan KOSTELECKÝ [3, 4] and Aleš BEZDĚK [1]

[1] *Astronomical Institute, Czech Academy of Sciences, CZ 251 65 Ondřejov, Fričova 298, Czech Republic*
[2] *Geological Institute, Czech Academy of Sciences, Prague, CZ 165 00 Praha 6, Rozvojová 269, Czech Republic*
[3] *Research Institute of Geodesy, Topography and Cartography, CZ 250 66 Zdiby 98, Czech Republic*
[4] *Faculty of Mining and Geology, VSB-TU Ostrava, CZ 708 33 Ostrava, Czech Republic*

**Corresponding author's e-mail:* jklokocn@asu.cas.cz

ARTICLE INFO

Article history:
Received 12 February 2025
Accepted 21 April 2025
Available online 6 May 2025

Keywords:
Gravity field models
Gravity aspects – Strike angles
Surface/subglacial topography
Subglacial volcanoes, Impact craters
Faults, Canyons, River valleys, Lakes
Groundwater, Paleolakes Paleoocean
Hydrocarbon occurrences

ABSTRACT

The traditional gravity anomalies are not able to describe subsurface density anomalies completely. The gravity aspects provide more detailed information. They are functions of the disturbing static gravitational potential (assumed to be available in the form of Stokes parameters). The gravity strike angles belong to a set of gravity aspects. They are surprisingly informatively rich; they inform about shallowly deposited ground density/ porosity anomalies and existing stresses. The gravity fields of the Earth, the Moon, and Mars are already known "sufficiently well" and thus, the gravity aspects have a chance to be successfully applied to study various geological features. For the Earth, it helped to confirm or discover impact craters, subglacial volcanoes, and lakes in Antarctica and Greenland or paleolakes in the Sahara. We discovered a correlation between the combed strike angles (aligned in one direction) and huge oil/gas deposits like Ghawar (Saudi Arabia) or the Caspian Sea; many other localities were tested later for potential hydrocarbon or groundwater occurrences. The gravity aspects yield a cheap remote sensing tool for testing various causative bodies (target deposits).

1. INTRODUCTION

The gravity aspects (descriptors) are functions of the disturbing static gravitational potential (which is assumed to be expressed in terms of spherical harmonic expansion). The classic gravity anomaly belongs among the gravity aspects; the gravity strike angles also belong to them.

Our motivation to write this summary (not a review) was the increasing number of our papers during last ten years about the applications of the gravity aspects (Klokočník et al., 2010, 2014, 2016, 2017a–c, 2018a, 2019, 2020a–f, 2021a,b, 2022b,c, 2023a–c, 2025a–c; Kostelecký et al., 2024; Mizera et al., 2022). The gravity aspects proved to be considerably more powerful in variety of geo-applications than the traditional gravity anomalies. We were surprised what the strike angles can disclose about subsurface structures (Klokočník et al., 2017b, 2018a, 2019, 2020b,f, 2021a, 2022b,c, 2023a,c, 2025a–c). Here we focus on the strike angles for specific geological features. We have, however, no ambitions for exhausting geological/geophysical interpretations, leaving this on specialists.

Our inspiration to introduce and use the gravity aspects for geo-applications became mainly from works of Pedersen and Rasmussen (1990), Beiki and Pedersen (2010), and Kalvoda et al. (2013). We gathered information from these and other sources and created a system of the gravity aspects (Klokočník et al., 2014) and the relevant software for a universal use. It is assumed that the global gravity field parameters (harmonic potential coefficients or Stokes parameters) are given and that they are already known, for a celestial body in question, with a "sufficient quality" (this term will be specified below).

The reader is referred to all definitions of the gravity aspects and various examples to our books (Klokočník et al., 2017a, 2020a) and to *Supplementary material* (SM1, formulae and Table 1) here. In the main text, we repeat minimum of theory (Sect. 2), but summarize our findings about the strike angles for various applications (Sect. 2.2, see also Klokočník et al., 2023a). The examples of the use of the strike angles are in Sect. 4.

We work with the following gravity aspects (SM1): (1) *(free-air) gravity anomalies* Δg (in fact the gravity disturbances, see the formula SM1:A2 without the second term), with (2) the *Marussi tensor* of the second derivatives of the disturbing gravity potential, A3, namely with its radial component T_{zz}, with (3) the *gravity invariants* I_1 and I_2 (A4-5) and (4) their specific *ratio I* (A6), a shape indicator of subsurface density anomaly, variations, of a causative body, energy resources, target deposit TD). Also, with (5) the *virtual deformations vd* and (6) with places having systematically one-way oriented ("combed") lines of the *gravity strike angles* θ (A7).

Cite this article as: Klokočník J, Cílek V, Kostelecký J, Bezděk A: Gravity strike angles to study various geological features. Acta Geodyn. Geomater., 22, No. 2 (218), 151–182, 2025. DOI: 10.13168/AGG.2025.0011

There are other similar functions like the gravity aspects (e.g., Pajot et al., 2004; Murphy, 2007; Murphy and Dickinson, 2009; Andrews-Hanna et al., 2012). They were used mostly for a local investigation (not with the harmonic geopotential coefficients of the global gravity field models). We have tested them (excluding those from Andrews-Hanna et al., 2012) and did not find them necessary for our research.

Pitoňák et al. (2017) introduced the third-order gravitational tensor, but for a practical use it would unfortunately suffer from a large noise. Ebbing et al. (2018) tested curvature components, derived from satellite gravity gradients, based on the GOCE satellite mission data (Gravity and Ocean Circulation Explorer, ESA), de facto various combinations of the components of the Marussi tensor – mean/minimum/maximum, and the Gauss curvature. Maximum and minimum curvature were combined to compute a shape index, a quantitative description of the shape of the local morphology. Ebbing et al. (2018) did not work with the EIGEN 6C4 and did not use the strike angles (known since 1990) nor the virtual deformations (known since 2012, defined by us, Kalvoda et al., 2013; Klokočník et al., 2014).

All the aspects are usually complicated non-linear combinations of the harmonic geopotential coefficients of the gravitational field models of the studied celestial bodies. The input to our analyses with the gravity aspects is given solely by the harmonic coefficients C_{lm}, S_{lm} (Stokes parameters, geopotential harmonics) to maximum degree/order (d/o), or L_{max}, of a static, global, comprehensive *gravitational field model*. It is computed from a huge number of various data (remote-satellite as well as terrestrial data in the case of the Earth, satellite-only for the Moon, Mars, Venus or Mercury), defining the disturbing gravitational potential (see SM1). Theory and software are tailored to this and only this input. We can, for example, reduce the free-air gravity anomalies to the Bouguer anomalies. We cannot, however, utilize such corrected anomalies to compute all other gravity aspects. We would have to return to the original C_{lm}, S_{lm}. In fact, we do not need and do not interpret the gravity anomalies.

The individual gravity aspects are sensitive in various ways to the underground lithological density contrasts (variations) and stress field orientation due to the causative bodies (density variations). Therefore, all used together provide more complete and thorough information about the ground density variations than solely the traditional Δg can do. The set of the gravity aspects provides information about location, shape, orientation, the tendency to 2D or 3D patterns of the causative body. It is remarkable that also stress tendencies and tensions, concerning various geological features, can be imprinted in and expressed by the strike angles, although the input data are always the same – the harmonic coefficients of a *static* gravity field model. Similarly, it applies to the virtual deformations.

There were and are different ways how to study the density variations (presence of the causative bodies) in geophysics. The traditional Δg, mostly Bouguer type, from gravimetric measurements, sometimes amended by T_{zz}, computed from gravimetric measurements or measured by the gradiometers, are in use for the local purposes (exploration geophysics, e.g., Donofrio, 1998; Grieve, 2005; Saad, 2006; Murphy, 2007; Murphy and Brewster, 2007; Murphy and Dickinson, 2009, and many more). For more references see *Sect. 2* in Klokočník et al. (2020a). The excess mass and the depth to the centre of mass are obtained from inversion of the gravity data along a vertical profile (e.g., Castaldo et al., 2014).

The traditional way has increasing competition in much more general view achievable by means of the full set of the gravity aspects, used together. The quantities Δg and T_{zz} also belong to the gravity aspects but are less important for our purposes. The most important are the strike angles (more in Sect. 2.2). They come out as remarkable, promising, admirable tool to study various geological features from the gravity field models of the celestial bodies (e.g., Klokočník et al., 2023a).

For areas of our interest, a combed (one-way aligned) structure with a parallel course of strike angles is typical (references above). These structures on the Earth indicate places where underground reservoirs or oil traps are not disturbed by later folding or fault tectonics. We were able to detect also subglacial volcanoes, trenches, surface and ground water or paleolakes in Sahara (Klokočník et al., 2017b,d, 2018a, 2020a,e).

Not to overestimate the role of the strike angles, we should be aware that in the inverse task as it is presented here (i.e. to derive density contrasts from the given C_{lm}, S_{lm}), one cannot achieve a unique result (one derives the whole integral of C_{lm}, S_{lm}, defining these coefficients, not directly density inside the integral). We need to implement further data, like magnetic anomalies, seismic data, topography, and others.

2. NOTES ON THEORY, DATA, AND METHOD

2.1. THE STRIKE ANGLES AMONG OTHER GRAVITY ASPECTS

The most important from all gravity aspects for this study are the gravity strike angles. The *strike angles* θ (strike directions) were defined as follows (Pedersen and Rasmussen, 1990; Klokočník et al., 2017a, 2020a, plus references therein; and SM1, with a special table-review, Table 1, with the information about significance of the gravity aspects):

$$\tan 2\theta = 2\,\frac{T_{xy}\left(T_{xx}+T_{yy}\right)+T_{xz}T_{yz}}{T_{xx}^2-T_{yy}^2+T_{xz}^2-T_{yz}^2} \qquad (1)$$

ambiguous within a multiple of π/2, meaning that the angle θ will only be estimated within a multiple of π/2, where T_{ij} are the components of the *Marussi tensor* $\mathbf{\Gamma}$ (see, e.g., Pedersen and Rasmussen, 1990), i.e., the

(a) *combed strike angles aligned in the studied area*
=one-way oriented strike angles
comb_factor→ 1

(b) *dishevelled strike angles*
= strike angles are in diverse directions
comb_factor → 0

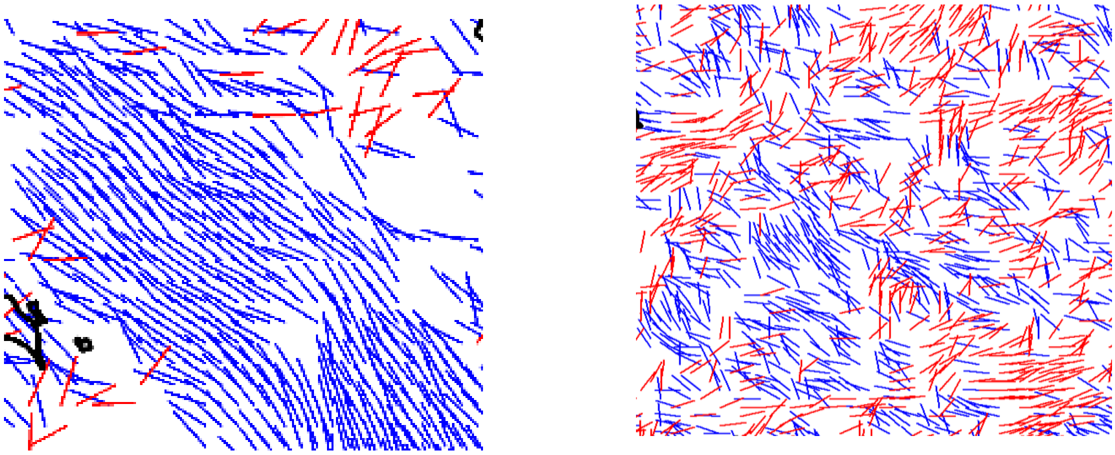

Figs. 1a–e We learn about the strike angles.

Figs. 1a,b Tutorial figures to Theory, SM1–3, and Table 1: the strike angles θ [deg]: (a) combed (here linearly aligned into one prevailing direction), and (b) chaotic.

tensor of the gravity gradients or second derivatives of the disturbing potential (see SM1, formulae A1, A3). There are 9 components of $\mathbf{\Gamma}$, just 5 of them are independent. These are non-linear combinations of the harmonic (geo)potential coefficients.

To the coordinate system for eq. (1) in Pedersen and Rasmussen (1990): let the measurement system be denoted by **X** (x, y, z) and let the rotated coordinate system be denoted by **X**'. The coordinate system **X** needs to be rotated around the *z*-axis to achieve the *x*-axis coinciding with the strike direction θ so that elements of the first row and first columns of $\mathbf{\Gamma}$ will be identically equal to zero. In other words (Murphy and Brewster, 2007): the strike angle indicates "how to rotate the measurement frame around the *z*-axis to align one of the *x*- and *y*-axes within the main directions of the ground structure. The expression for θ is obtained by rotating the coordinate system around a vertical axis to minimise the sum of squares of the three components of the gravity gradient tensor $\mathbf{\Gamma}$ that involve a derivative in the *x*-direction."

Mathematically, the strike angle θ eq. (1), (A7), can be the main direction of the tensor $\mathbf{\Gamma}$ (under certain condition), so it is an important direction. This direction is general in space, it depends on all three types of T_{ij} components (x, y, z) as we can see from (1). Not surprisingly, it can be important also geo-physically (or better "planeto"-physically). They provide evidence of the anisotropy, e.g., about the target material in the case of impact features; they react on porosity changes, first on shallow layers, and then on their background (anything), more below in this section. They are connected with "stresses". We can say that $\mathbf{\Gamma}$ relates to stress anisotropy. More about θ is in Sect. 2.2**.** The examples of their applications for the Earth, the Moon, and Mars are in Sect. 4.

Besides $\mathbf{\Gamma}$, there are the gravity invariants (SM1: A4, A5), independent of any rotation. The invariant I_1 is the sum of the six products of two tensor coefficient matrix elements, a nonlinear functional model with regard to the geopotential harmonics, while I_2 is the determinant "det" of $\mathbf{\Gamma}$. The invariants are filters enhancing sources with big volumes (Pedersen and Rasmussen, 1990); they discriminate major density anomalies into separate units, spots.

Pedersen and Rasmussen (1990) showed that a specific ratio I of the invariants I_1 and I_2 (A6) [values of I being always within the interval <0,1>] has an interesting geophysical meaning. If the causative body is flat, theoretically 2D, then I equal zero ($|\mathbf{\Gamma}| = 0$). The higher I, the more 3D-like source is. A pancake or a sphere? In the case of the oil/gas deposits we rather expect flatter (pancake or umbrella-like) than spherical objects, i.e., rather "smaller" ratio I (say<0.3) than prevailing high values of I (say>0.9). For a slope or top/caldera or vicinity of volcano, we should expect $I \rightarrow 1$. The strike angles react on the density variations in depths from hundred metres to a few kilometres (in a big contrast to the gravity anomalies, which may go much deeper). With I<0.3, emphasizing flat causative bodies, we "penetrate" only shallowly beneath the surface, while with I<0.9 we can "see" a bit deeper (compare Fig. 1c to Fig. 1d). It is difficult to say "how deep" without additional information.

Note that (1) the ratio I from Pedersen and Rasmussen (1990) provides the condition necessary but not sufficient, and that (2) this criterion is not the only one possible criterion to detect flat TD bodies; for another see, e.g., FitzGerald and Holstein (2014).

(c)

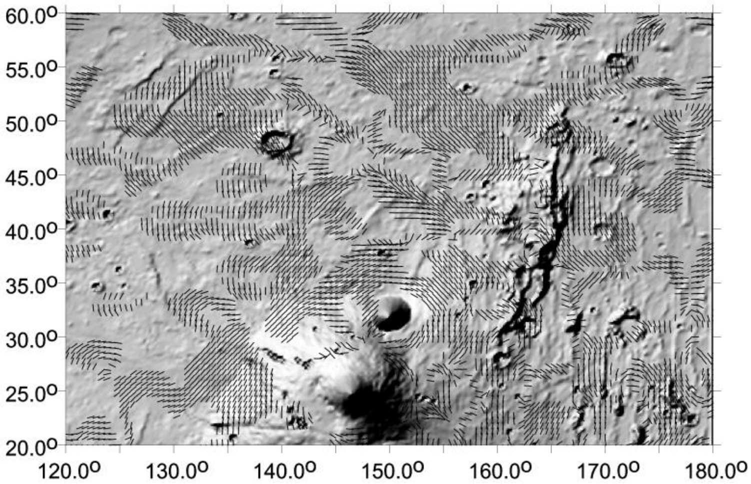

(d)

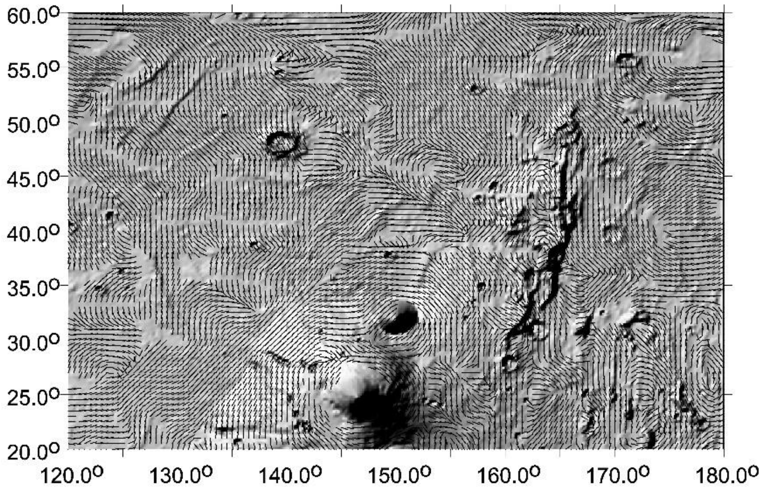

Figs. 1a–e We learn about the strike angles. For more figures see SM2: 12, 19-21, and 38.

Figs. 1 c, d The strike angles θ [deg], a comparison between them for the ratios (c) I<0.3 and for (d) I<0.9. See theory above and in SM1. This example is for the hypothetical northern paleo-ocean on Mars near Elysium volcano; from (Klokočník et al., 2023b). The 3D-shaded topography from the altimeter MOLA [m] is added. With I <0.3, emphasizing flat causative bodies, we "penetrate" shallow beneath the surface, while with I <0.9 a bit deeper. With $I \leq 1$ we would fill the figure with the strike angles everywhere; it would happen on volcanoes, trenches, and nearby.

There are works about a relationship of maximum degree L_{max} of the gravity field models and effective depths of the causative bodies to study the structure of geological features; the most recent paper was written by Goossens and Smith (2023), and is related to Δg. We note (using theory in SM1) that the relevant effective depth for the gravity strike angles θ will be much lower (the causative body is closer to the surface) than Δg (it follows from the comparison of the gravity aspects in the model case, see *fig. 2.1* in Klokočník et al. (2017a) and a paragraph about the simulation tests in Sect. 4).

If the underground density variation source is close to 2D, then one component of the stress field has the direction of the strike angle θ, the second is directed to the centre of the central body and the third lies in the direction of the gradient of the gravitational field. However, a reasonable geodynamic interpretation of the meaning and value of the strike angle θ depends on the knowledge of the regional or local tectonic regime.

The strike angles are generally oriented chaotically, i.e. in various directions. Sometimes, however, within a certain area, they are systematically aligned into one prevailing direction. The alignment along the studied structure, e.g., fault (along the long axis of the fault) discloses existing stress trends. Then we say that strike angles are linearly *combed* (Figs. 1a,b). They also can form a circular *halo* ("aura") around the impact craters or other circular-like features ((Fig. 1e and Figures in Sect. 4). The alignments have various physical reasons (see below, Sect. 2.2).

We have developed empirical criteria to characterize a degree to which θ are aligned (Kletetschka et al., 2022; Klokočník et al., 2019). We defined the *Comb* factor (Sect. 3), *Comb*=1 for perfectly combed strike angles, 0 for not-combed; more is below and in SM1.

(e)

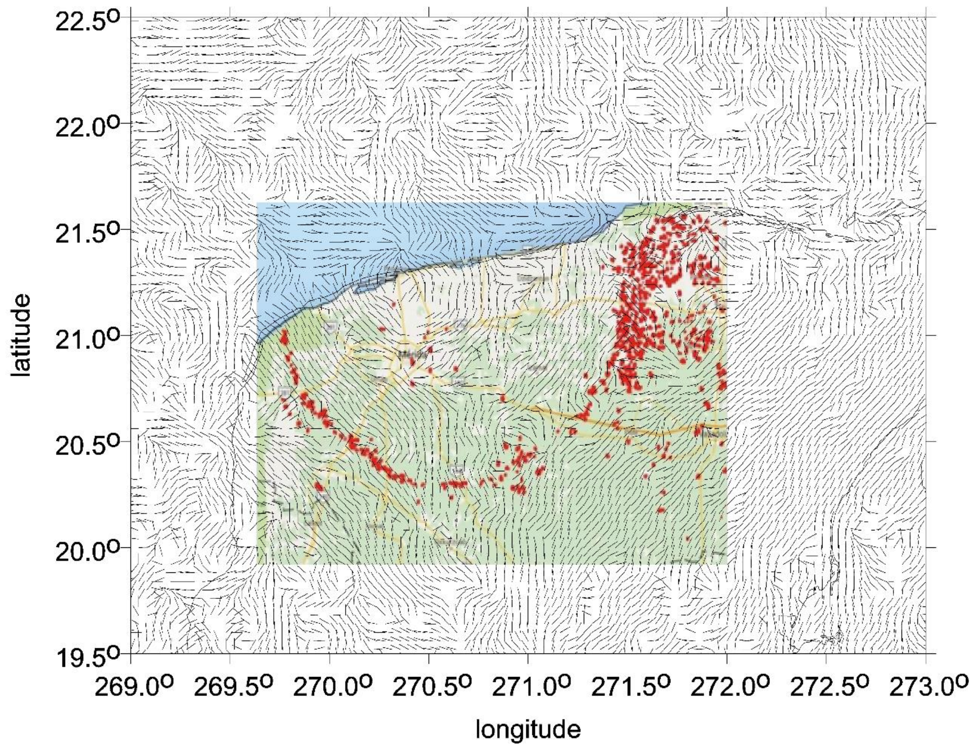

Figs. 1a–e We learn about the strike angles. This is the end of the lecture in the main text. For much more examples see SM2–4.

Fig. 1e Tutorial for this section, but also for Sect. 4.1.2.1 about Chicxulub, North Yucatan, Mexico: the strike angles θ are "combed" into a (semi)circular "halo" around the impact crater (over land only). Yellow: roads. The crater Chicxulub is not exposed on the surface; it is beneath sediments, and its northern half is in shallow waters. The EIGEN 6C4 gravity field model used. A large area around the crater with highly aligned θ is affected by the impact event generating post-impact changes concerning oil/gas, coal, hydrocarbon deposits, (ground)water or sinkholes (Mayas' cenotes) – red dots. Such consequences depend on size of crater (in turn on energy of the impacting asteroid) and on the regional material in situ before the impact event; Klokočník et al. (2020a, *Sect. 6*). They can be far-reaching (thousand kilometres from the impact). About a half of the impact craters known in Northern America possesses economic minerals (e.g., Donofrio, 1998; Reimold et al., 2005), see also James et al. (2002), and Sect. 4.1.2.

The following axioms (*i*, *ii*), although may seem trivial, should be mentioned:

(*i*) Warning against "short-cuts": The gravity data only indicate geologic structures (anticlines, faults, salt domes, etc.), any of which may occasionally contain concentrations of target deposits (TD) of various practical minerals, permafrost, hydrocarbons, ice, or water. The combed θ are *not* directly due to gas, oil, coal, minerals, or water content.

(*ii*) Correlation (here between the gravity aspects and locations of TD) does not imply causation. Indication is not proof.

Nevertheless, there is so many indications and examples of the correlation that it cannot be by chance (our examples are in Sect. 4 and in our works cited above). The alignment can be related to (ground)water, faults, river valleys, paleolakes, sediments and other porous material, or hydrocarbon occurrences.

2.2. *THE STRIKE ANGLES – NOTES TO THEIR PHYSICAL MEANING AND INTERPRETATION POSSIBILITIES*

The combed (aligned) strike angles θ bear information about a higher porosity, about changes of porosity/density and stress fields connected with various geological features and processes. There is a plenty of such observations and applications discovered till now (for examples see Sect. 4 and SM2). Here we have a few comments.

Note 1: after the impactor's explosion and during the post-impact evolution, the strike angles may have changed their original pre-impact direction. Due to the impact event, there is a change revealed by the strike angles while the other gravity aspects do not react (e.g., negative Δg or T_{zz} inside the crater, both positive in the rim; fragmented extremes of I_1 and I_2 around the crater, negative *vd* inside). The strike angles inside and around the crater become significantly combed, sometimes providing evidence about the direction of deformations. They seem to be parallel to the weakness in the strength of the rock, e.g., direction schistosity and or presence of faults or micro-fault zones. The impact event energy is imprinted into the gravity aspects. There may be even no crater (but an airburst). The release of the energy of the impactor may trigger stress in the rock along the cleavage planes while the stress perpendicular to these planes is preserved (probably the cases of Saginaw Bay and Tunguska events, see the examples in Sect. 4). This internal anisotropy is what is being detected by the strike angles.

Diverse post-impact influences and changes may reach large distance from the source crater. The bigger impacting body, the more energy and thus the bigger crater, the more intensive and extensive consequences which remain written into the strike angles. The impacts enhance porosity and permeability in rocks of all parts of the impact structures and around it, sometimes to large distances (see the strike angles in SM2, slides 9, 13-14, 16-17, for Mexico, the whole Yucatan, in the area of Mexican Gulf west of Yucatan, or Veracruz, also in sea). The consequences can be, for example, a triggering mechanism to move rocks/minerals from deeper layers to the surface (e.g., Vredefort or Sudbury S2: 27-29). The impacts may lead to crustal deformation and deposit extensive blankets of material local-dependent ejecta with economic minerals and hydrocarbons (e.g., Donofrio, 1998; Reimold et al., 2005; James et al., 2002). The cenotes/sinkholes (karst features, the case of Chicxulub in the local limestone, Fig. 1e) may be sparked off as a good example of post-impact phenomena. These long-reaching effects should be studied further on.

Note 2: the combed θ can be used as a *preliminary diagnostic tool* for further exploration of sites with TD (Klokočník and Kostelecký, 2014; Klokočník et al., 2021a). Important to note that no specific digging is required to apply this method. The method helps to decide to exclude or include the region from more detailed later investigation, based on the traditional data and procedures, thus potentially saving money for drilling on the spot.

Note 3: Rivers, canyons, faults, groundwater or ice, permafrost on the Earth (regolith on the Moon), paleo-lakes, oil/gas deposits, sedimentary layers, mud – their appearance is signalled by the combed (aligned) strike angles θ, and, in a specific way, by the other gravity aspects. There is not only a reaction to a higher porosity of that place in comparison with its surroundings, but also reaction to certain flows, such as slope movements or land-sliding, tensions, stresses, forces connected with a genesis and evolution of such features.

The strike angles are plotted as projections into the horizontal plane and the strike lines indicate the deformation patterns associated with mass density variations. We used θ to investigate stress fields, generated by geomorphic processes and events appearing on various localities including the state during collisional orogeny between the Indian and Asian lithospheric plates in the Nepal Himalaya here in (Sect. 4.1.3.9.).

There is another "stress tensor" important for understanding geodynamic processes, such as global plate tectonics, earthquakes or for the management of geo-reservoirs and underground storage sites for energy. A worldwide map of the maximum horizontal stress is under the auspices of Heidbach et al. (2018). The theory speaks about three components of the stress tensor (but this is not "our" Marussi tensor). Their relationship to the gravity strike angles θ (which is a 1D quantity) is not known.

Note 4: Reservoir source rocks are porous and absorbent, and can be saturated with water, oil and gas in various combinations. They should thus provide contrasting (higher) porosity, and relatively lower density, with the relevant changes in the gravity signal in a form of the gravity aspects as they are known for lower density causative bodies on the Earth (depending on the background beneath the sedimentary layers). A similar situation can be expected on Mars (Klokočník et al., 2023b) as for the ground water or sediments (possibly bearing hydrocarbons). Potential hydrocarbons are more likely to be found in places with ordered combed structures, which probably represent places with linear (uniform) water flow (as on the Earth) that would carry (water lift) and concentrate hydrocarbons in suitable places, e.g., under impermeable clay layers. The examples are in Sect. 4.3, taken from (Klokočník et al., 2023b,c). More and more applications are coming (e.g., Kadirov et al., 2023; Özsöz and Oruç, 2023; Eppelbaum et al., 2024).

2.3. DATA

Gravity, magnetic, and topography data. The input data to our analysis are the harmonic geopotential coefficients (Stokes parameters) of the spherical harmonic expansion of the disturbing gravitational potential, nothing else. All the formulae in Supplement about Theory (SM1) clearly document the dependence of all the gravity aspects on the geopotential coefficients, i. e. on the global gravitational field characteristics. The surface (for Antarctica subglacial) topography comes from networks of heights above a reference surface, gathered from satellite or airplane measurements. The magnetic anomalies – namely the values of magnetic induction – as an additional informative source to the gravity data/aspects are available, were used in our analyses for the Earth, the Moon, and Mars, but they are not discussed here.

The Earth: We make use of a high quality, of the highest accessible precision worldwide and of the highest resolution *combined gravitational models*, based on satellite and terrestrial data; now it is still the *EIGEN 6C4* (*E*uropean *I*mproved *G*ravity model of the *E*arth by *N*ew techniques). It is a global but detailed gravity field model which includes gradiometry data from the whole *GOCE* mission (*G*ravity field and steady-state *O*cean *C*irculation *E*xplorer, ESA); Förste et al. (2014). This model is expanded to maximum d/o = 2190. It corresponds to the ground half-wavelength resolution 5x5’ [arc minutes, arcmin] or equivalently ~9 km on the Earth’s surface (SM1). We have tested, among others, also an experimental XGM2019e gravity field model (Zingerle et al., 2019) but found no profit for our goals, comparing the XGM to EIGEN 6C4. Precision of EIGEN 6C4, expressed in terms of Δg, is ~10 mGal, but in many civilized land areas and over the oceans and open seas it can be much better (SM1). The authors of EIGEN 6C4 did not have access to most of the recent high resolution terrestrial gravity data on the continents, thus they took a synthesized gravity anomaly grid based on EGM2008 (Pavlis et al., 2008a,b; 2012). That means that the errors for the high d/o harmonic coefficients in EIGEN 6C4 are dominated by the relevant errors in EGM2008. It is evident that the accuracy varies with latitude and longitude. The EGM2008 does not contain the GOCE data. EIGEN 6C4 represents about one order improvement in the ground resolution and accuracy of the geoid over EGM 2008, mainly in the polar areas. The terrestrial data base of EIGEN 6C4 is based on that in EGM 2008 (with some additional, new data collected by GFZ, Germany), in turn, on the data gathered by the National Geospatial-Intelligence Agency, USA. Pavlis et al. (2008a,b, and private comm.) presented maps with the accuracy of Δg (among others), derived from the variance-covariance matrix from the least-squares adjustment of the harmonic coefficients (we reproduce example in SM1, p.10).

Topography data. ETOPO 1 was used (Amante and Eakins, 2009). It is a part of the global 1’ relief model of the Earth surface that integrates land topography and ocean bathymetry from a large number of satellite and other measurements. Its precision is ±10 m in heights (but not everywhere). [Now we work with its improved version ETOPO 22.]

Bedmap 2 is a basic *subglacial topography* data set valid for Antarctica (Fretwell et al., 2013). It contains the bedrock elevation beneath the grounded ice sheet. It is given as a 1x1 km grid of heights of the bedrock above sea level. The actual spatial resolution is worse, 5x5 km, but often worse.

We also worked with the *RET 14* (Hirt et al., 2016), a degree-2190 gravity field model *SatGravRET2014*, given as a set of harmonic geopotential coefficients, meaningful only for the continent of Antarctica (not globally!). Roughly speaking, it combines the global gravity field model *EIGEN 6C4* and the Bedmap *2* topography. More precisely, the RET 14 combines predecessors of EIGEN 6C4 to d/o=180 with other and very important gravity data sets. These gravity models describe the long- and medium-wavelength components of the Earth’s static gravity field from GRACE and GOCE missions. The “non-gravity” data to RET 14 comes from the *Earth 2014* one arcmin global topography model (Hirt and Rexer, 2015) which incorporates the Bedmap 2 bedrock topography and the other data sets; these are topography from the Shuttle Radar Topography Mission (SRTM), Greenland Bedrock Topography v3, and SRTM30_PLUS v9 bathymetry. A full account of the construction of Earth 2014 and RET 14 is provided by Hirt and Rexer (2015). RET14 increases resolution of underlying gravity field models and decreases resolution of Bedmap 2; the spatial resolution of RET14 should be about 10 km over the whole Antarctica (excluding the polar gap and a few areas with no or rare data in Bedmap 2).

As for the independent data, Egyptologists cooperated with us and provided locations of archaeological sites, defining the former living places at playas or lake/river banks. This information was important to check our estimates of the paleolakes’ locations and extent. The archaeological data were used for delineating boundaries of the acceptable living conditions (like the access to potable water) during specific epochs (Klokočník et al., 2020e).

We also applied (see, e.g., in Klokočník et al., 2020d) magnetic intensities from the magnetic field model EMAG2 (a global 2-arc-min resolution grid) compiled from satellite, marine, aeromagnetic and ground magnetic surveys (source: Maus et al., 2009).

The Moon: We use the gravity model GRGM1200A (Lemoine et al., 2014) to d/o = 600. The formal precision of GRGM1200A should be ~10 mGal. The surface topography of the Moon comes from LOLA (Lunar Orbiter Laser Altimeter) on board of the LRO (Lunar Reconnaissance Orbiter). The heights are given relative to a reference radius of 1737.4 km. A nominal precision of the LOLA altimeter heights is ~10 cm.

Mars: We use the gravity model JPL JGMRO_120 F (Konopliv et al., 2020) to d/o = 80. The global surface topography is derived from the MOLA (Mars Orbiter Laser Altimeter) on board of the MGS (Mars Global Surveyor). The accuracy should be ~1 m radially and ~100 m horizontally.

3. METHOD

We compute all the gravity aspects (as defined in SM1, A2-A13), magnetic intensities where available, and topography. We make use of our software (Sebera et al., 2013), of our co-workers Bucha, Kostelecký, and Bezděk and partly software developed by our colleagues (Bucha and Janák, 2013). Numerical stability of computations of all gravity aspects should be guaranteed to d/o ~ 10 000 (Bucha, priv. commun., 2020). We used the Mercator-Marine projection for all pictures excluding the polar zones where we apply the orthographic projection.

The gravity disturbances are shown always in milligals [*mGal*], the second order derivatives in Eötvös [*E*]. Recall that 1 *mGal* = 10^{-5} [ms^{-2}], 1 *E* ≡ 1 Eötvös = 10^{-9} [s^{-2}]. The invariants have units I_1 [s^{-4}] and I_2 [s^{-6}]. Negative values are in all these cases as well as for surface/subglacial topography in blue colour, positive in red (may be a bit unusual to see green colour in the middle of colour scales, i.e., for the values around zero).

The strike angles θ [deg, ^{0}] are angles (A7), not vectors. We plot them as short abscissae of the same length everywhere, in a regular network. It does not mean that in the real world something like as a regular net of tensions exist: geological and geophysical lineaments are never of a constant or identical length, and neither are they separated by uniform distances. It is good to repeat and emphasize that θ yield 1D information only, i.e., the horizontal component of the main direction of Marussi tensor. The strike angles proved to be very useful in geo-applications (see above Sect 2,2, or, e.g., Klokočník et al., 2023a).

We plot also pixels with different colours for different values of the *Comb* statistical factor to express a degree of the alignment (the *Comb* values are between 0 and 1). We work with the *Comb* factor according to (Kletetschka et al., 2022 and SM1). For the point *P* in question, we select points B_i around *P*. The "comb coefficient" in *P* is then equal to the weighted mean value of the scalar product of the unit vector in *P* with the unit vectors in B_i. The *Comb* factor lies always in the interval <0,1>. For ideally aligned (combed, correlated, parallel) vectors from the surroundings of the point *P* considered in the relevant analysis, we have *Comb* = 1. The scalar product (cosine) is "flat" around zero, thus *Comb* $\geq$0.99 is selected for a "perfect correlation".

In order to show the halos around the craters, we draw θ in the horizontal plane, as an angle rotating from East towards North. (It means for example that the SN direction has azimuth 90^0 to west.) It is a change from our papers published before 2022, where the reference direction was North (the local meridian). It does not mean any change in physics, but the interpretation must account for this change. For example: the strike angles are aligned (logically) along the long axis of a fault not perpendicularly to it; the strike angles create evident halos (rings) around the craters, etc. Sometimes we prefer black and white drawings for all directions of θ. It is a good choice for example for the craters. For colourful versions of figures with the strike angles, the following is valid: red means the direction to the north from east and blue means the direction to the south from east.

Note also that density of data of the strike angles can differ. For the Earth, for example, we can use the default density of 9 km (corresponding exactly to max d/o=2190 of EIGEN 6C4), but we can emphasize the structures by using the strike angles using 4 km, or 2 km distances of the lines of θ, depending on the local conditions and details intended to show.

To illustrate the shifts represented by the virtual deformations *vd* (A8-A13), the semi-axes of deformation ellipse *a* and *b* are computed in their relative size. The *vd* [-, = dimensionless] is geometrically expressed by its dilatation (shown everywhere in our figures in red colour) or compression, contraction (in blue). The area with dilatation of the ellipse of deformation have a high potential energy. Thus, there is a trend to move energy to areas with contractions, compressions. The examples about volcanoes or craters with their rings are in Sect. 4.

The user should not forget to work with all the gravity aspects for the area of interest. The gravity aspects are mutually interrelated, especially θ, *vd*, and T_{zz}. Together they may disclose more than only one of the aspects. Sometimes the interpretation queries appear when for example θ and *vd* show different trends, e.g., perpendicular directions of stresses. The user should know the regional/local geology.

Where it is possible, we compare our results with independent geological and geophysical data. Further to the gravitational data (magnetic intensities, topography…) are always welcome to strengthen our deductions. It can be, however, problematic. It will be demonstrated on the maps of terrestrial gravity anomalies for known deposit sites for oil/gas not used in EIGEN6C4. The reason for a potential problem is simple – one cannot fully rely upon these terrestrial sources. Sometimes a part of data is not published intentionally, may be classified and unavailable, or out of the range of such maps (boarders of various state).

4. EXAMPLES

We begin with regions with known geology to approve our method. We compare what is known from various terrestrial data to our results. Then we extrapolate to other places. The results presented here have, in majority cases, already been presented in our previous papers. We add *Supplement*s with many figures, SM2 for the Earth, SM3 for the Moon, and SM4 for Mars, although the Moon and Mars are nearly omitted in the main text. We want to document the universal character of the gravity aspects. Several our papers and one book deals with the Moon and Mars (Klokočník et al., 2022 a,c, 2023a-c, 2025c).

The typical gravity signals in terms of the gravity aspects for various geological features are summarized in Table 1 (this section). Let us take the impact craters/basins as an example. The most common and conspicuous signature is a circular gravity low in the floor of the crater. For simple bowl-shaped craters, gravity data indicate that the anomaly is largely due to the presence of an interior allochthonous breccia lens. In big complex craters, the main contribution is from fractured parautochthonous rocks.

The most interesting is the comparison of the different gravity signals of impact craters on the Earth and on the Moon or Mars. Craters on the Moon, generally speaking, have a wide range of signals because meteorites originally struck the surface of the still-hot Moon, smashing through it and causing the crater floor to be flooded with volcanic rocks. Gradually, as the lunar crust cooled, smaller craters formed, as well as multi-ring structures and the usual type of craters that form in already solid rocks. In this case, we observe especially on the Moon intense landslide movements and sometimes indications of another wider ring around the craters. On the Earth, the impact structures form complex circular and oval formations that influence tectonic and possibly

Table 1 A comparison of the gravity aspects typical for crater/basins, mascons, volcanoes, faults or waters, based on our experience from the Earth, the Moon, and Mars.

feature	Δg	T_{zz}	θ	*vd*
bottom of crater	negative	negative	combed	compression
bottom of basin	negative	flat around zero	combed	compression
around crater/basin			halo	dilatation
centre of volcano	positive	positive and strong	no signal	dilatation strong
around volcano	negative	negative and strong		compression
inside mascon	positive	flat and small	combed	dilatation
closely around mascon	normal		normal	compression
faults	negative	negative	combed	compression
water, ground water, paleolakes, oil/gas	negative	negative	combed	compression in, dilatation nearby

volcanic regime of the entire region including the formation of long trenches. On Mars and the Moon, the gravimetric signal helps to distinguish older circular structures that are now to some extent overlain by sediments or material ejected from younger meteorite impacts.

The values of Δg and T_{zz} are negative inside the crater changing positive and negative values for the rim(s) and between them. The gravity invariants have extreme values inside and around the crater and they are concentrated in the rim(s). The strike angles θ often exhibit orientation in one prevailing direction near the crater and encircle the crater as a halo. The virtual deformations *vd* inside the crater show compression; the rim(s) is/are surrounded by dilatation (and the space between the rims is again compression). If the crater is large and has a central peak, we can detect it by positive T_{zz}; if the crater is huge (crater basin), the central peak can "grow" to a mascon caused by upward motion of the regional material. The magnetic signature of craters is more varied with the main effect being a magnetic low due to a reduction of susceptibility after the impact.

Simulation studies. We recall (but will not repeat) our synthetic (simulation) tests showing the effectiveness of our method (for technical details see Klokočník et al., 2010, their Sect. 4.4. about the impact craters Chicxulub and Popigai; Klokočník et al., 2017b, *fig. 7*; Klokočník et al., 2018a, their Sect. 3.6, or Klokočník et al., 2021a, for the case of paleolakes in Sahara, Lake Vostok in Antarctica and oil/gas deposits). We also mention our tests of various and dangerous artefacts in the gravity field modelling, a warning against possibility of the false results due to the imperfect data or their processing (Klokočník et al., 2021b).

4.1. EXAMPLES FOR THE EARTH

4.1.1. TEST AREAS

4.1.1.1. CZECH REPUBLIC

The relatively small territory of the Czech Republic (CR) is one of the best geologically explored territories in the world, mainly due to the long period of prospecting for mineral resources, including gold and uranium deposits (Chlupáč et al., 2002). In addition to conventional geological methods, the territory is also explored by geophysical methods, including airborne gravimetry at scales of 1:50 000 to 1:200 000. It is, therefore, tempting to compare the local terrestrial gravimetric measurements with the gravity anomalies computed from EIGEN 6C4, and to observe behaviour of the other gravity aspects, what they can show for such a territory.

Always we should work with the full set of the gravity aspects; for CR see SM2: 3-6**.** In terms of strike angles, our observations follow. Figure 2a combines the gravity disturbances Δg, together with names of several cities in CR, with the strike angles θ and shows how much they are combed, e.g., in West Bohemia (western part of CR) in large zones with surface coal mining and valley (see also item 3. below). Figure 2b shows *vd*.

1. The faults in NW-SE direction, roughly parallel to the Tornquist Zone, are significant. [Note that The *T*rans-European Suture *Z*one is the lithospheric boundary between the Precambrian East European Craton and the Phanerozoic orogens of South-Western Europe]. The faults probably reflect process of coalescence of Europe from different micro-blocks. In the northern part of CR, they are represented by several approximately parallel lines of the so-called Sudeten faults. We can there distinguish the long

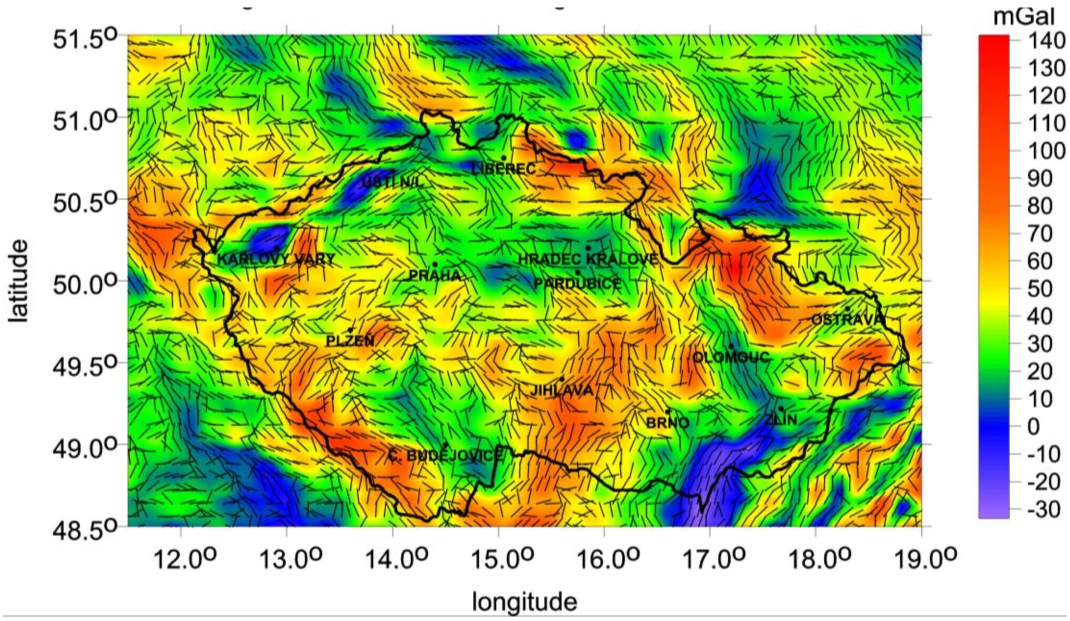

Fig. 2a The gravity disturbances Δg [mGal] from EIGEN 6C4 for the Czech Republic, and the strike angles θ [deg], I<0.9; strongly combed areas (NW) correlate with coal deposits.

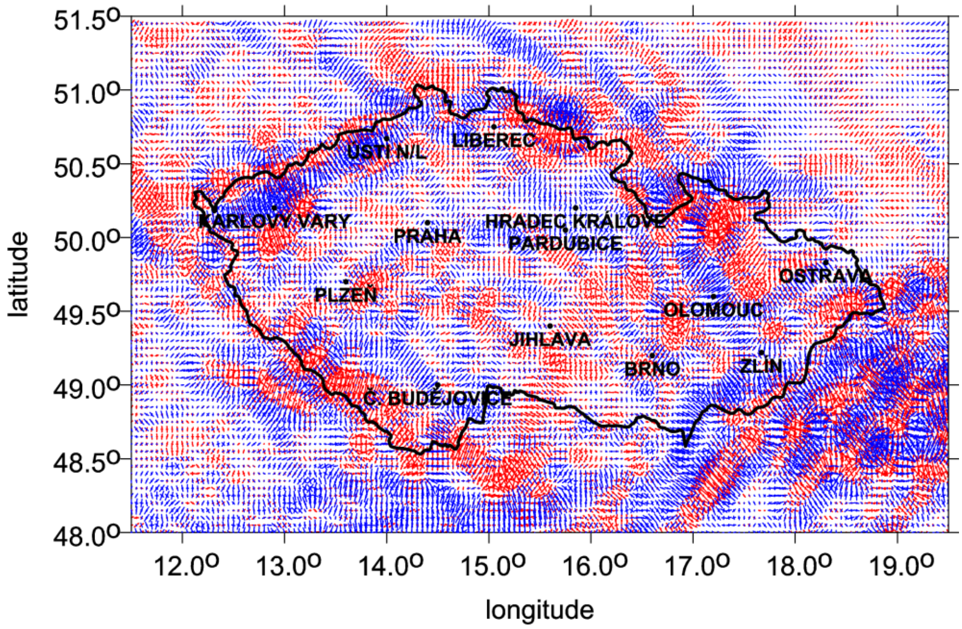

Fig. 2b The virtual deformations *vd* [-] for the Czech Republic; dilatation (red), compression/contraction (blue). By comparing Δg, θ and *vd*, we get a nice example how the conventional gravity surface measurements often cannot be sufficient for geological and geophysical aims. For more figures about Czechia see SM2:3-6.

Lusatia Fault and the Elbe Zone extending towards Meissen. On the south-western border of CR, we can see fault zones parallel the south-western border of CR.

2. The second major trend is the NE-SW fault system, which is represented mainly by the Cenozoic rift structure of the volcanic hills of the central České Středohoří. Parallel to this much younger geological structure is the system of deep faults of the Carpathian system (Peripieniny Lineament, northern part of Vienna Basin) in the easternmost part of the territory and especially in Slovakia (east of the CR).
3. In addition to linear structures, we can observe block structures, which usually correspond to crystalline, often granitic cores of the protruding mountain ranges such as the Krkonoše (mountains in the north of CR), the Nízký Jeseník mountains (east-north), the Kralický Sněžník (east, E), Šumava (hills in the south, S) and parts of the Waldviertel or the Slavkovský les.

4. The strike angles document homogeneous block of the Czech Cretaceous Basin in the northwest of CR and zones parallel to the Alpine and Carpathian foredeep. The course of the Vltava (Moldau) river follows the N-S direction quite closely, which is also more prominently represented in the more easterly Blanice Furrow (Blanice is name of a river). The strike angles here indicate a deep basement of the Vltava direction (river Moldau in Czech language), although only shorter local faults have been found by the conventional geological mapping.

4.1.1.2. ISRAEL

There is a good knowledge about the gravity and magnetic fields in Israel from terrestrial sources (e.g., Sneh et al., 1998; Eppelbaum., 2018*)* for a comparison with remote sensing data. EIGEN 6C4, namely the virtual deformations derived from it, were used for regional tectono-geophysical zonation (both qualitative and semi-quantitative) in the Arabian–NE Africa region (Eppelbaum and Katz, 2017; Eppelbaum et al., 2018). An integrated tectonic map based on the examination of satellite and terrestrial geophysical-geological data and containing structural features of different ages has been constructed. It can serve for physical-geological models and to search for useful minerals.

Figure 3a shows Δg and labels for the individual geological structures known from terrestrial investigation. We confirm how well EIGEN 6C4 reproduces the known facts, their position and extent. Figure 3b shows v*d* in a wider area, including Israel, NE Egypt, Sinai, and east Mediterranean Sea. The compression in the Dead and Red seas and dilatation around are remarkable. Cyprus has significant dilatation, also positive Δg and T_{zz} (see additional figures in SM2). The strike angles θ [deg], I<0.9, highly combed along the faults, but also on many other places, including oil/gas mining sites are in Figure 3c.

The strike angles are organized along the long axes of the faults in a conspicuous way. This zone is not any exception, it is rather a rule (see Theory, Sect. 2). The same effect has been observed for the Lake Baikal, Lake Vostok, Great Canyon, trenches east of Japan, deep part of valley of the river Nile (see SM2: 44, 76, 78) or catenae (chain of craters) on the Moon (SM3: 22, 27).

At first glance, from Figures 3b,c we can derive that the choice of calculation methodology strongly influences the resulting pictures and the possibilities of geological interpretation. That is, it suppresses or highlights certain features and a different representation may do the same with different structures. Therefore, we always try to compare multiple representations. In particular, Figure 3b shows the very prominent Read Sea and Dead Sea rift triplet, the outcropping Golan Heights Block, the NE Jordan Block, and to a lesser extent the Sinai and Egyptian Eastern Desert. In addition, there is a continuation of the Anatolian and Aegean faults around Cyprus and the southern coasts of Turkey and Greece. If we could see only Figure 3c, we would probably dismiss it. But Figure 3c shows well stress fields aligned along the long axis of all the presented faults. Again, we observe that the individual gravity aspects yield different views on the same reality due to their different sensitivity e.g., to depth of causative bodies.

4.1.2. IMPACT CRATERS

The strike angles help to understand impact processes and deformations in the impact craters and their surroundings. The impact craters often bear economic minerals, like gold or uranium at Vredefort (South Africa), diamonds in Popigai, Kara (Russia) or Ries (Germany), hydrocarbons at Chicxulub (Campeche Bank, Cantarell oil fields, Mexico), Ames, Avak, Calvin, (USA), Boltysh (Ukraine), or copper and nickel in Sudbury (Canada). Quoting from Grieve (2005, pp. 22-23): “The largest impact structures have the greatest probability of having significant economic resources. These are the most energetic events; they affect the largest volumes of target rocks, have the largest post-impact hydrothermal systems and form the largest topographic basins…”. The strike angles confirm and can indicate new such perspective localities. James et al. (2002) wrote: …70 % “of the 60 craters host energy resources such as oil, gas, coal, uranium, mercury, critical and major minerals as well as hydropower resources.”

4.1.2.1. CHICXULUB

The literature about Chicxulub impact crater, Mexico, Yucatan, is rich; we chose a few examples: from Alvarez et al., 1980; Smit et al., 1980; Hildebrand et al., 1990, 1995….to Goderis et al., 2021. The crater Chicxulub is huge, not exposed (diameter 170-250 km) and the effect of this impact on the Earth was far-reaching, global, as is well-known. Klokočník et al., (2010, 2025a) argued that Chicxulub may be a double-crater.

The strike angles combed around Chicxulub to a halo were shown in Figure 1e. The haloes following the craters’ rims are strong on land, although the crater is not exposed on the surface. The ring of cenotes (sinkholes, originally potable water sources used by Maya), one of the post-impact effects and consequences, agrees well with the halo created by the strike angles along the outer, most compact ring of the crater. Cenotes then continue in a cluster on the east edge of the crater (see SM2: 11-12).

We show θ in a wider zone around the crater in Figure 4 (and in SM2: 8, 9, 11, 13-15, together with other gravity aspects). Tertiary sedimentary layers of the flat northern Yucatan outside the crater have, as expected, linear and also highly combed θ. A contrast of the density of sediment or a changed porosity (with respect to surrounding rocks) is high enough to be gravitationally distinguishable. The cenotes as well as oil/gas deposits near Yucatan (S2: 16-17), although epigenetic, are not there by a chance (e.g., Grieve, 2005, p. 21).

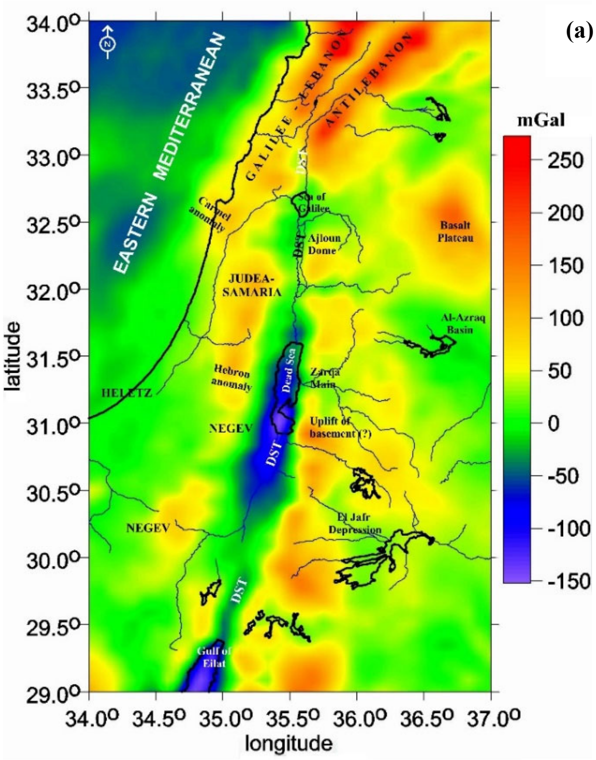

Figs. 3 a,b,c Israel and eastern Mediterranean Sea:
(a) enlargement for Δg [mGal], with names of various geological features (credit L. Eppelbaum); see also SM2:49,
(b) *vd* [-], negative (compression) inside the faults, see also enlargements in SM2:49,
(c) the strike angles θ [deg] highly combed along the faults.

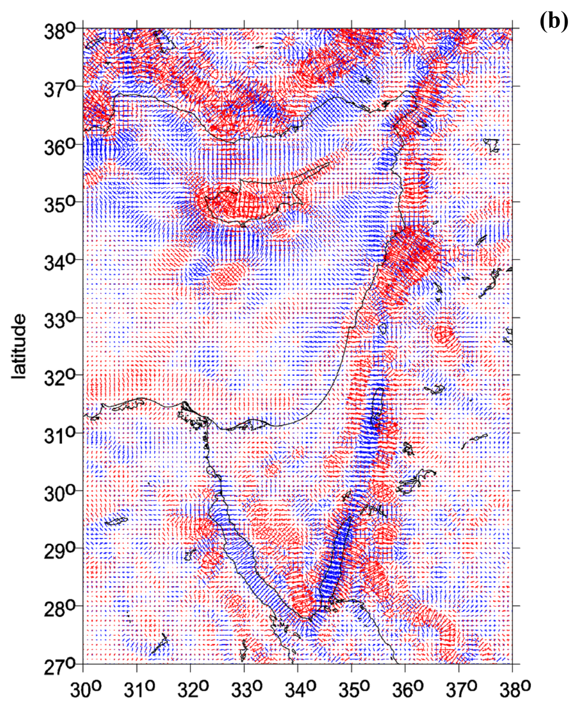

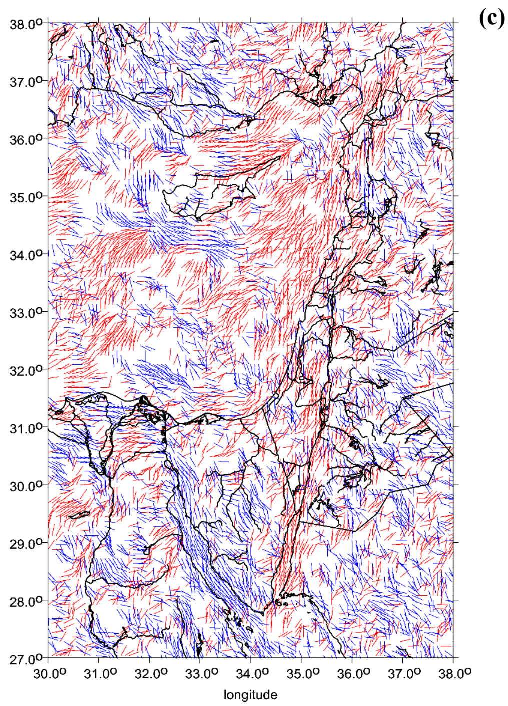

Let us recall Donofrio (1998) who wrote: "Seventeen confirmed impact structures occur in petroliferous area of North America, nine of which are being exploited for commercial hydrocarbons… Disrupted rocks in proximity to impact structures, such as Chicxulub in the Gulf of Mexico off Yucatan, also contain hydrocarbon deposits". James et al. (2002), p. 40, wrote: "…There are several craters that host fossil fuels, with the submarine Chicxulub impact crater…" and "A total of 21 craters have oil/gas/hydrocarbon/coal resources, of which 19 host oil and gas." Figure 1e and further figures in SM2 demonstrate a halo around the central part (min. two rings). Figure 4 complements Figure 1e, showing the strike angles for Chicxulub together with the gravity anomalies. The strike angles are also strongly linearly combed far from the crater, mainly SW-NE (due to the local high porosity around and the cenotes outside the rims of Chicxulub E of them). The question is whether this can indicate the direction of incoming impactor/s (impacting asteroid/s), Klokočník et al., (2020b).

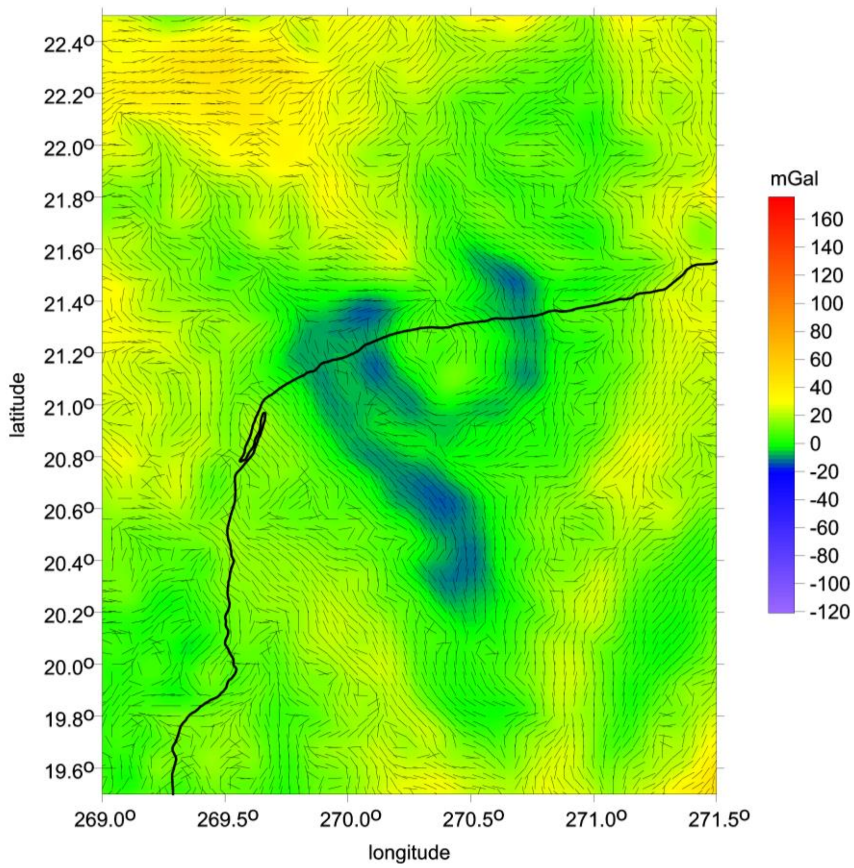

Fig. 4 The strike angles θ [deg], I<0.9, together with the gravity anomalies Δg [mGal] for Chicxulub. Compare to zoom in Figure 1e which contains also cenotes (sinkholes in the local limestone), one of the post-impact effects.

The tail of negative anomaly in the SN direction in the southern edge of the crater and linearly combed strike angles also in this SN azimuth (Fig. 4 and slides 8-15 in SM2) probably belong to the crater event (syngenetic feature), but there is no definitive conclusion attainable via only the gravity data, without the other data. Together with the impact circular structures, linear structures, "the impact grabens", can be generated. In the case of Chicxulub and Popigai structures, we studied them in a detail (see our new paper Klokočník et al., 2025a).

4.1.2.2. VREDEFORT

Vredefort Dome is a huge (250–280 km in diameter), very old (2 023 ± 4 million years, Proterozoic) impact basin in South Africa. The Vredefort structure represents exploited polymetallic deposit area (e.g., James et al., 2002, their *Table 1, fig. 1*).

We reproduce the strike angles θ (black) together with the second radial derivative T_{zz} (colour) from Beiki and Pederson (2010) based on local airplane measurements. We prefer this older figure to EIGEN 6C4 which does not show the halo so perfectly (probably because of poorer terrestrial gravity data available for that area in EIGEN 6C4).

In Figure 5, we can see: *(i)* a typical halo from the combed strike angles around the crater along its rims, the alignments coinciding with the positive values of T_{zz}, *(ii)* a central peak expressed in both T_{zz} (positive value) and appearance of θ (linearly combed values), *(iii)* an overall trend of linearly combed θ (probably indicating the direction of the incoming impactor).

Moreover, *(iv)* in the SE direction of the main crater, there is another, much smaller circular feature (Fig. 5 right down). It has negative T_{zz} inside and positive around, and a halo from the strike angles around. It is looking like an actual crater, a simple crater with a small central peak. It may be an additional crater. It would not be surprising to have more than one crater connected with the main and biggest one. After such a huge impact event as Vredefort was, hardly can sit there only one crater as one isolated feature. From astronomical point of view, it is reasonable to assume a cluster of craters after such enormous event. Vredefort is very old; the smallest remainders near the main crater may disappeared from the surface meantime. It would be a good example that also the gravity signal is "getting old", eroding, abrasion due to course, sometimes being affected by faulting and plate motions.

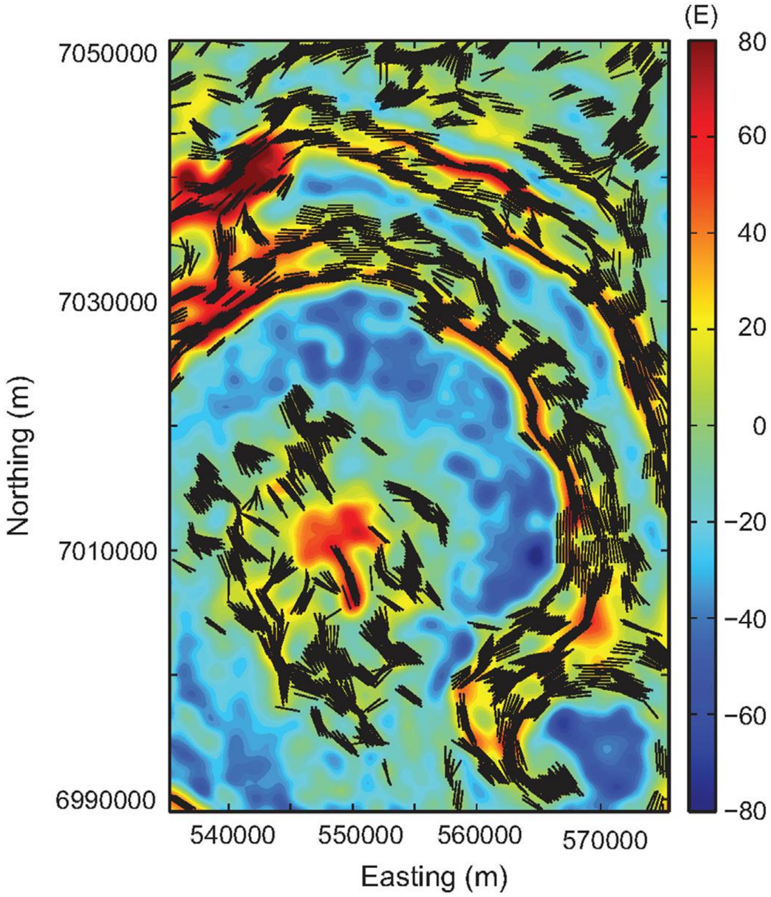

Fig. 5 The strike directions θ [deg] with dimensionality I<0.3 and T_{zz} [E] plotted together. Credit: Beiki and Pedersen (2010). Note the halos around the crater basin, a central peak and linearly combed θ around it.

4.1.2.3. RIES

The prevailing opinion is that the ~30 km-diameter Nördlinger Ries and the 4–8 km-diameter Steinheim feature (~40 km SWW of Ries) in limestone plateau of southern Germany represent a double-crater. But Buchner et al. (2022) argue (not for the first time and not without critical voices) that the age of Ries and Steinheim differs and thus that we deal with two independent impact events.

Dating impact craters is a problem. The impact creates mixtures of rocks of different ages and the impact itself causes major changes, including evaporation or selective melting of rocks. In the case of the two impact craters Steinheim and Ries, we encounter both the original idea that it is a composite impact (e.g., Sturm et al., 2013) and the model of the formation of two independent craters (Buchner et al 2022 and their older papers). However, it is unlikely that two impact structures of different ages would lie close to each other. In addition to Ries, note the orderly geological orientation in the northern part of the image and the more chaotic structure in the lower half of the image, where the influence of active Alpine arc is more pronounced (Figs. 6a-c).

Figure 6a shows *vd* around Ries. One can see a typical situation: compression inside the crater, in a contrast to dilatation around it (the rim) and in the direction from the Steinheim to Ries. The latter observation may be important for our understanding of the evolution of the Steinheim – Ries configuration. It corresponds to the geologic findings that of the impactor came from SW-NE. It also agrees with ejecta directions, a wide angle from Ries to E, ES, EN, with famous tektites (moldavites; vltavíns in Czech language) found mostly in the southern Bohemia (Czech Republic).

Figure 6b shows the strike angles combed linearly, roughly in the SW-NE direction, i.e., from Steinheim to Ries. Around Ries, they are combed into a halo. The halo is not perfect (being dominated by something else than the crater's event on the SE and NE sides).

In Figure 6c, we can see again the strike angles, but computed and plotted with a finer network of EIGEN6C4 data, trying to show more details (with a bit higher danger that we show artefacts). Steinheim is small but detectable – see the change of direction of the strike angles in its vicinity (Fig. 6c). Further supportive figures are in SM2: 30-32.

We can say a little about the age of these features using solely the gravity data; we cannot decide definitively whether these objects are two separate craters of different age or one double-crater. The smaller size and hence a lower impact energy did not

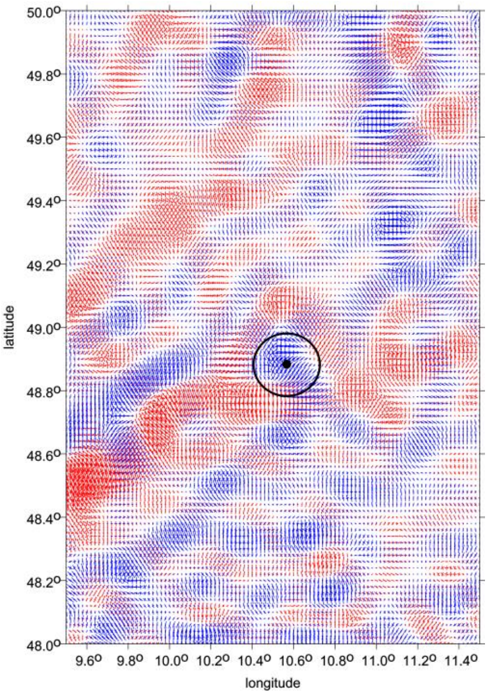

Fig. 6a The virtual deformations *(vd)*[-] with EIGEN 6C4.

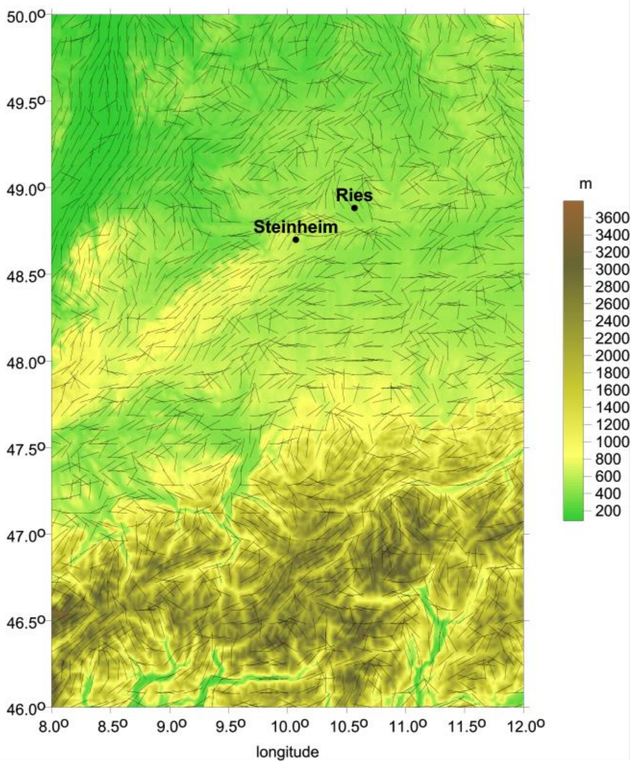

Fig. 6b The strike angles θ [deg] (for I <0.9) with EIGEN 6C4, together with the ETOPO 1 topography [m].

create the Buntesbreccia rim at Steinheim, and neither the strike angle schemes indicate a distinct structure. On the contrary, the predominant features of the gravimetric record are structures related to the Alpine arc foredeep and probably a fault parallel to the Rhine rift strike.

Based on our results, we would say that the impactor came from SW, created the double-crater, first Steinheim and then Ries, with that well-known "fan" of ejecta (vltavíns). Thus, we support the majority opinion.

4.1.2.4. SUDBURY BASIN

Sudbury crater is an old, large, geologically well-studied impact crater near the Great Lakes (Ontario, Canada), to which mining of a number of ore raw materials (copper, platinum, palladium, gold or impact diamonds) has been bound for several decades. Nearby (~NE of Sudbury crater), there is a smaller, younger (independent) crater called Wanapitei, filled by water. Sudbury is significant polymetallic deposit area. This is a phenomenon relatively common in larger craters, related to the deep disturbance of the underlying rocks that has opened the way for, in some cases, subvolcanic activity, and in the others, hydrothermal solutions that leach or precipitate ore and other minerals. Post-impact tectonic motions are responsible for its oval shape.

Figure 7a shows T_{zz}, Figure 7b θ, I<0.9; the crater is clearly and typically marked. No surprise. The crater's bottom has small value of T_{zz} (in this scale we cannot observe the central peak), the rim around has positive T_{zz}. The strikes θ manifest alignment into a form of imperfect halo (around Sudbury as well as Wanapitei). The other gravity aspects show, what is

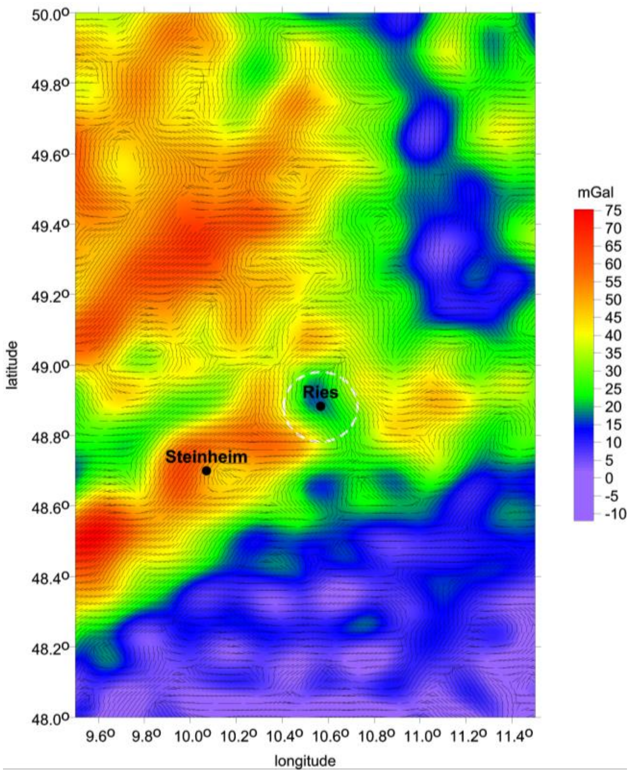

Fig. 6c is an enlargement for Ries and Steinheim with θ (a finer network of data generated from EIGEN 6C4 is used) and with Δg [mGal].

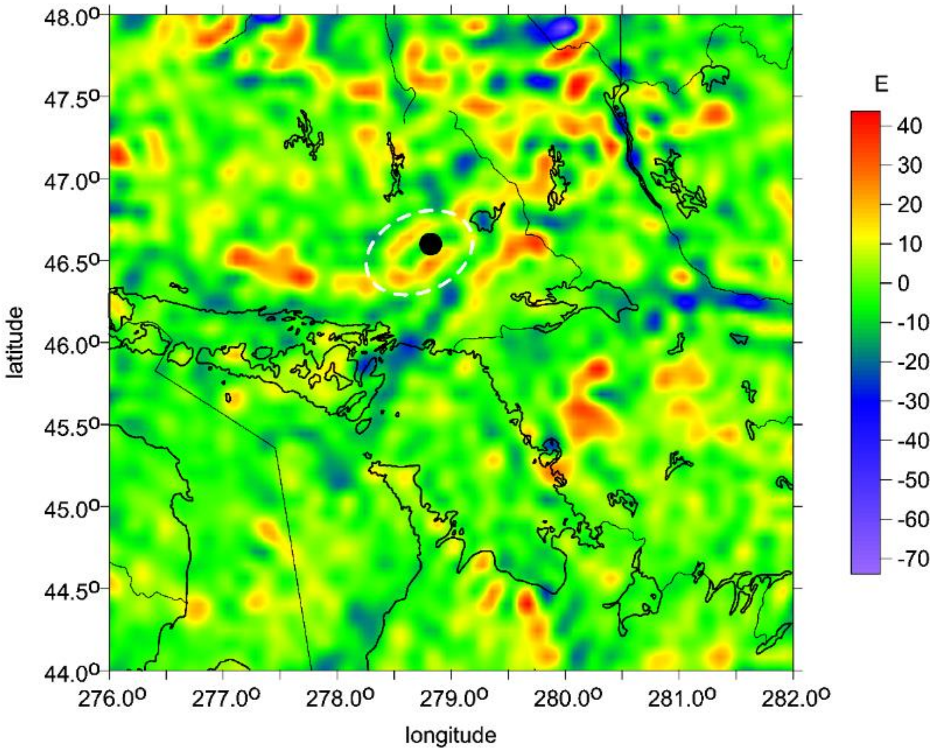

Fig. 7a T_{zz} [E] for the area around Sudbury near the Great Lakes. Crater's bottom long axis is about 70 km.

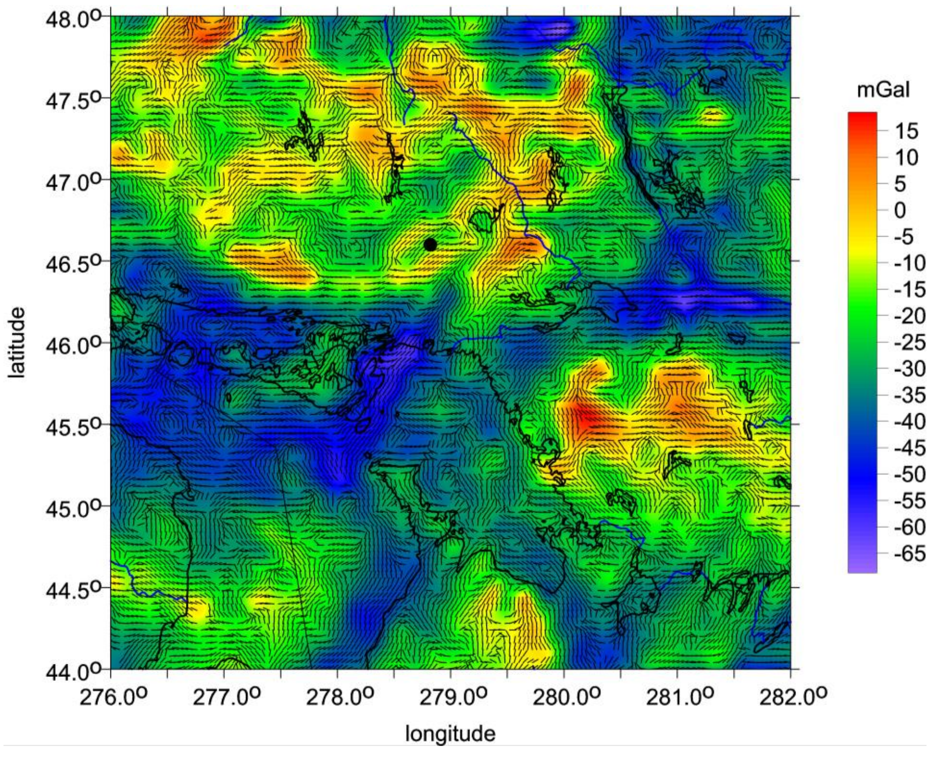

Fig. 7b The strike angles θ [deg] and gravity disturbances Δg [mGal] for the area around Sudbury.

expected for a typical impact crater, the depression in term of *vd* inside and dilatation around the crater; more figures can be found in SM2.

4.1.2.5. POPIGAI

This large, proved, exposed impact crater (diameter about ~100 km) is in Siberia, Russia. The impact generated the occurrences of minute diamonds. Nearby, in SSW direction, another, not yet proven crater, a circular feature known as Kotuykanskaya, is located (see Klokočník et al., 2020c with further references in; see SM2).

Popigai may be a multiple crater, a la catena, rare of the Earth (Figs. 8a,b); it was suggested in Klokočník et al. (2010) via the analysis of Δg and T_{zz} based on the older US gravity model EGM 2008. The most interesting feature of the crater structure is the existence of a long trench-like structure (blue colour in Fig. 8a) southeast of the crater. In particular, its northern part, adjacent to the crater, has some features of another possible crater. It cannot be ruled out that in this case we are confronted either with a multiple impact or with an activation of older fault structures. Figure, 8a shows gravity anomalies from EIGEN 6C4, recalling the possibility that Popigai (Popigai I) is really a multiple crater (Klokočník et al., 2010) and indicating direction of the impactor (Klokočník et al. 2020b), i.e., SE-NW or vice versa (see also Khazanovitch-Wulff et al., 2013).

Figure 8b is a zoom for θ (I<0.9), step 4 km, in the main crater Popigai with a halo created by the strike angles, with a mark of the central peak. More figures can be found in SM2.

Popigai crater is known for occurrences of aggregates of diamonds, sometimes up 1 cm large. They tend to retain the appearance of graphite or original organic aggregates. They are bound to outcrops of original rocks with an admixture of graphite or coal substance. It is absent in the central part of the crater, where the pressure and temperature were too high for diamonds to form or preserve (see, e.g., *fig. 1* in Masaitis 1998). Vishnevskyy and Montanari (1999) presented a diamond occurrence map (their *Fig. 6*) showing a more or less chaotic distribution caused by both an irregular admixture of carbon-rich impacted rocks and a complex, multiphase crater evolution.

4.1.2.6. *SAGINAW BAY EVENT*

The impact locality without any crater? The explosion (of a comet or its part or of porous asteroid) may happen in the atmosphere (Wittke et al., 2013) or on the ice cover or both (Wolbach et al., 2018; Firestone et al., 2001, 2007).

Let us mention the hypothetical impact locality at the Lake Huron in Michigan (Fig. 9a). There is a hypothesis that this structure may have been initiated during the onset of the Younger Dryas period about 12 800 cal years BP [calibrated years before present]. The ice cover, up to 2 km thick, which was there at that time (majority opinion), together with a few small craters, might be removed later within the subsequent deglaciation. The ejecta from the Saginaw Bay event is deposited, according to Davias and Harris (2015) mainly in S&N Carolinas.

It is easy to verify independently on the others that there is no clear sign of the impactor in terms of all the gravity aspects (see SM2) – meaning no crater. There is an oddity for the strike angles. If θ really can describe pressure trends, then we can read from Figures 9b,c that there is an arch or two arches or a semi-halo in W, S to ES from the Bay, similarly (but not perfectly) as are halos around the actual impact craters. The geologic data (see references concerning Saginaw Bay in Klokočník et al., 2019) suggest that the impactor direction would be NE/SW. It fits to Figure 9b, too. Figure 9c is a zoom of 9b and is more convincing about the halo/arcs. It provides more general view. Figure 9b shows θ (I<0.9) for a wider region. There is an extensive area of linearly combed strike angles in Iowa (and nearby). Could such relatively small crater like Manson (diameter about 35 km, located at 42°35′N, 94°33′W, hidden under surface) create something large like this belt (in SW-NE direction) more than 200 km long? This area is known for anomalous ground water supplies. The hypothetical impact disrupted granite, gneiss, and shales as well as sedimentary formations giving the rest of Iowa hard water and anomalous soft old water.

We did not use any geological data in our analysis for Saginaw, we only added our findings from the gravity data to already existing discussion, see, e.g., Davias and Harris (2015, 2022 with many references) in favour of the impact origin of Saginaw structure. Boslough et al. (2012) argue against it. Pinter et al. (2011) even wrote ‘a requiem for the Younger Dryas impact hypothesis’. Our work (Klokočník et al., 2019) was criticized by Schaetzl et al. (2019) but we got a chance to reply (Klokočník et al., 2020g).

In a big contrast to Δg and T_{zz}, showing no crater – this is well-known fact – confirmed by us (SM2), the strike angles from EIGEN 6C4 brought a new information. The strike angles may change their pre-impact orientation due to the explosion, while the other gravity aspects may remain more or less untouched. What we show in Figures 9b,c is a trace of a high pressure due to the impacting body falling roughly from NE.

Very interesting is to compare our remote sensing results (Figs. 9a-c) with independent terrestrial data, *fig. 3.3*, p. 43 in Wood and Harrison (1998), as for the geological faults and their orientation, see S2: 39. They agree well; the direction of the strike angles south of the Saginaw Bay is nearly the same as the direction of the faults.

Our results confirm a possibility of extremely intensive airburst, inwritten into the strike angles, not detectable by the other gravity aspects! The strike angles may here reflect a non-typical impact event on thick layer of ice (that later after the impact had ebbed). They tell us that the airburst, which would

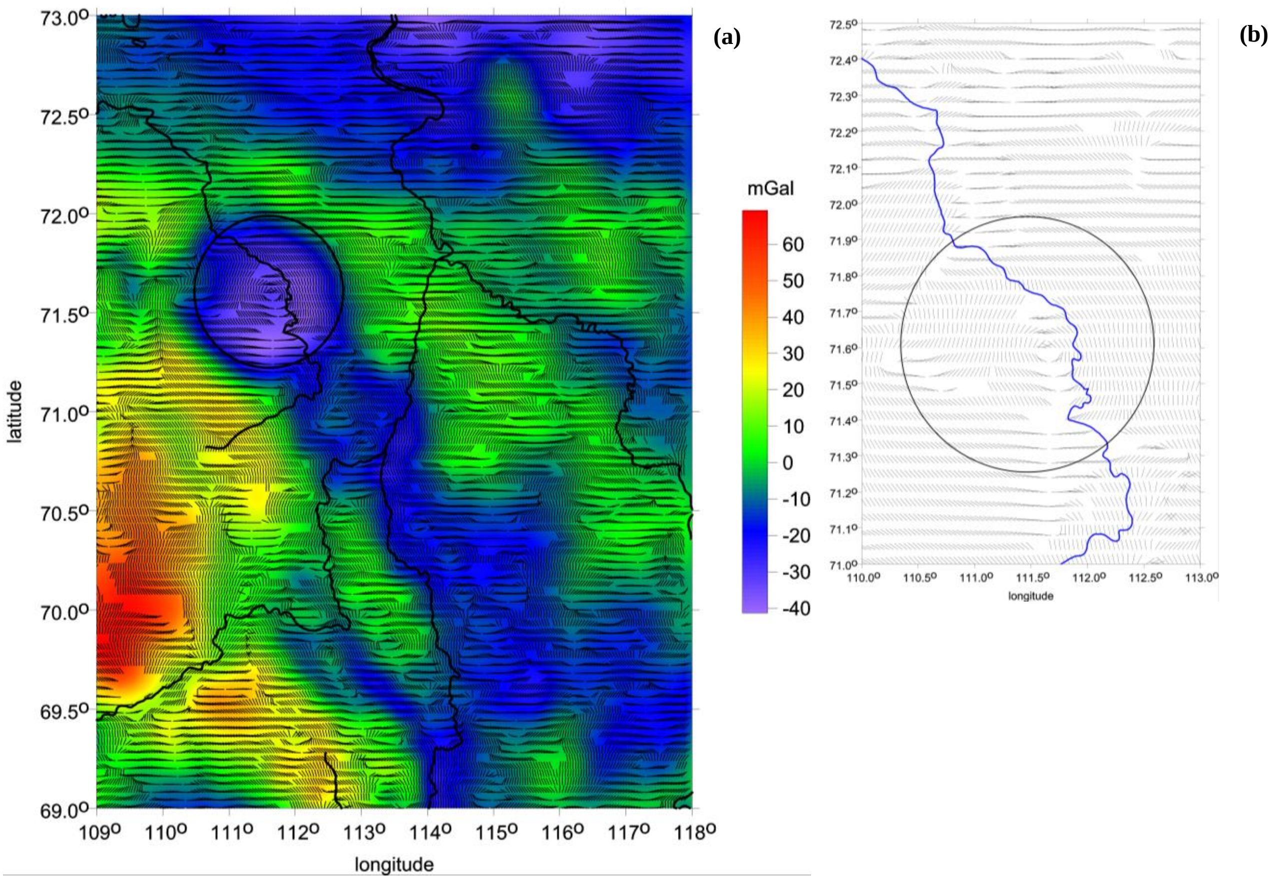

Figs. 8a,b Popigai, Siberia: **(a)** Δg [mGal] and θ [deg], $I < 0.9$; **(b)** details for θ in the main, largest and proven Popigai crater. A postimpact river (blue) disrupted the halo by erosion.

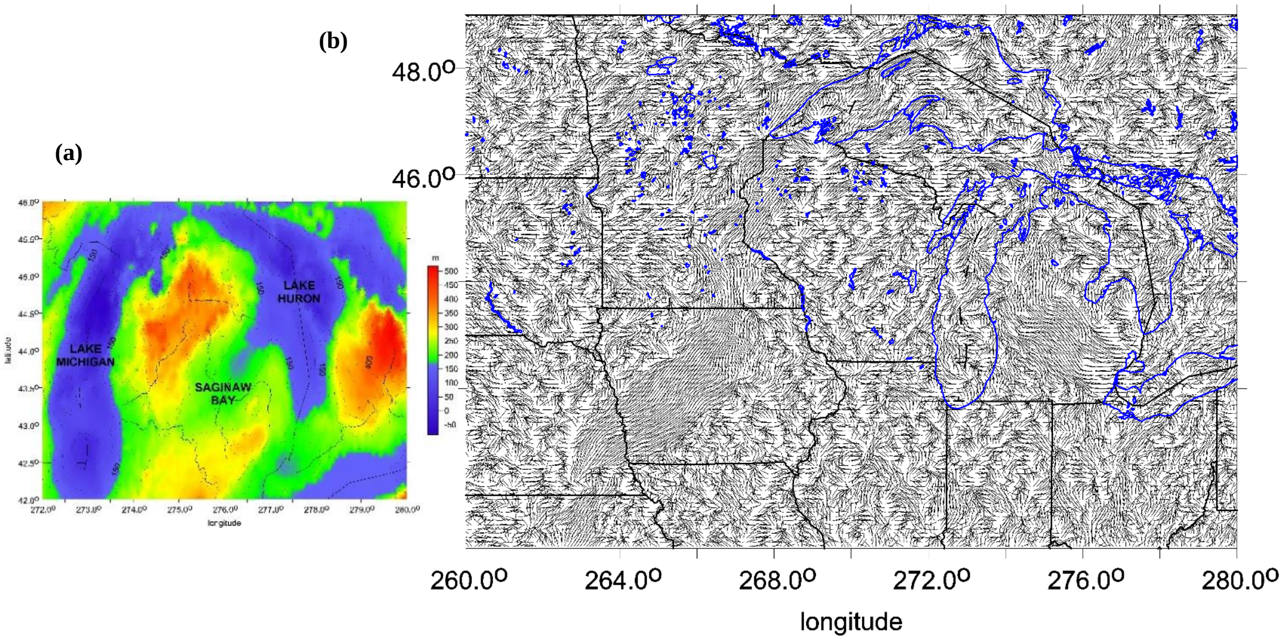

Figs. 9a,b **(a)** inset to the main figure: where is the Saginaw Bay (Lake Huron, the Great Lakes, USA and Canada); topography of that area from ETOPO 1 [m]. **(b)** the strike angles θ [deg], I<0.9, black and white, at the Great Lakes, Michigan, Iowa, and Nebraska.

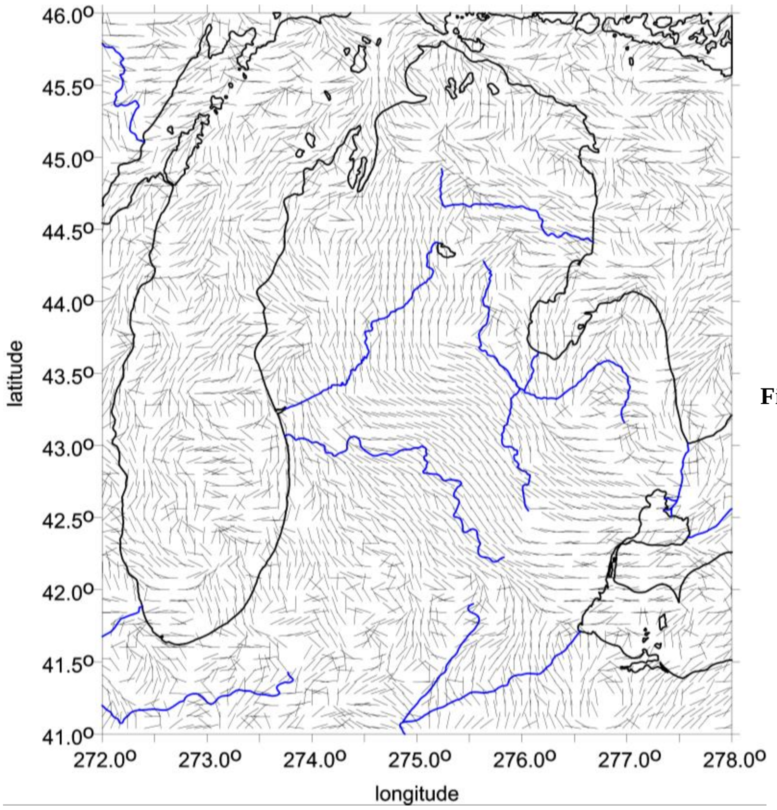

Fig. 9c Zoom for θ close to Saginaw Bay; two lobes of the combed strikes SW and SE of the Bay. One may imagine a semi-halo from SW to SE opposite to supposed direction of the hypothetical impactor (from NE). For the comparison with the independent terrestrial results see Wood and Harrison (1998), their *fig 3.3.*, p. 43

drastically affect Northern America – and in fact the whole world, was possible. The discussion about the Saginaw Bay event continues (e.g., Davias and Harris, 2022), no requiem.

The Tunguska event might be similar to the Saginaw case – an airburst, but much less powerful; thus, a similar effect on the strike angles (their alignment partly into a halo) is not so convincing for Tunguska as for Saginaw (more in Kletetschka et al., 2019).

Several circular structures, not-yet proven impact craters, were also studied. These are: (i) Kotuykanskaya (Siberia), already mentioned (Klokočník et al., 2020d); (ii) sub-glacial huge structure in Wilkes Land (Antarctica) – putative impact basin (von Frese et al., 2009, 2013; Klokočník et al., 2018b, 2020a); (iii) hypothetical crater Burckle on the deep bottom of the Indian Ocean (Klokočník et al., 2022b); (iv) hypothetical crater in Badain Jaran Desert (China), possible parent (source) crater for Australasian ejecta-tektites (Mizera et al., 2022; Karimi et al., 2022). Always the combed strike angles were helpful in such studies.

4.1.3. SUBGLACIAL VOLCANOES/LAKES, OIL/GAS DEPOSITS, PALEOLAKES, GROUND WATER

4.1.3.1. HYPOTHETICAL VOLCANOES AND LAKES NEAR THE LAKE VOSTOK, ANTARCTICA

The Lake Vostok (LV) is a huge subglacial lake in east Antarctica with fluid water in about 3.5 km depth. We reported about LV and our discoveries of two subglacial volcanoes nearby (Klokočník et al., 2016, 2017c) and three subglacial lakes (Klokočník et al., 2018a) between LV and Gamburtsev Subglacial Mts (GSM; east Antarctica, west of LV, on top in Figures 10a-10c) by means of the gravity aspects. Further, on the eastern rim of LV, series of further possible volcanoes can be located but they escape confirmation because of insufficient resolution of the gravito-topography model that was available (RET14, Hirt et al., 2016; Sect. 2.3.2).

Figure 10a shows the subglacial topography from Bedmap 2 (Fretwell et al., 2013). The LV is a depression, oriented NS (left-right on our figures), about 200 km long, up to 70 km wide, about 1 km deep (deeper in its southern part). Figure 10b shows the virtual deformations. LV is a compression zone, the two possible volcanoes (encircled) have dilatation “inside” and compression around them (typical for volcanoes everywhere, see Table 1). Note also “the lake district” behind the hill in west direction of LV, then continuing to the high GSM (top of this figure).

Figure 10c is for the strike angles θ, I<0.3, (together with the Bedmap 2). The prevailing alignment in the area is SN and its character inside LV differs from outside, it is more systematic inside; one can see that θ are perfectly combed. In the northern part of LV (in this figure on the right side), the pressure changed direction to NW and then back to N.

There is obvious connection between high GSM, a lower “lake district” east of it, and topographically lowest LV. The θ and *vd* studied in a detail in (Klokočník et al., 2018a) indicated a possible connection between GSM, the Lakes and LV throughout subglacial rivers.

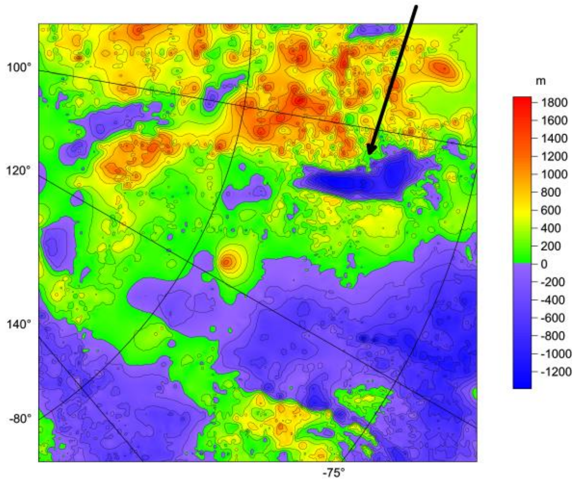

Fig. 10a inset on left: where is the Lake Vostok (LV, in east Antarctica), see the arrow. The subglacial topography of that area from Bedmap 2 [m];

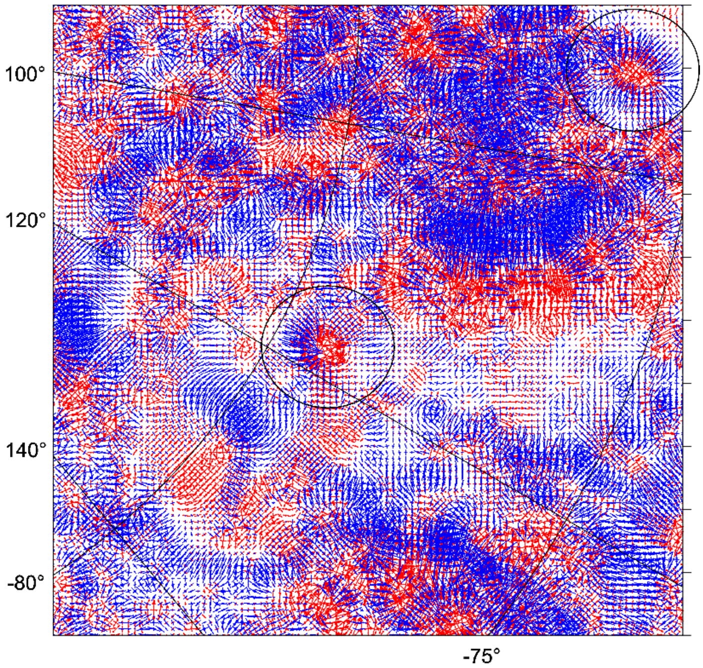

Fig. 10b the virtual deformations *vd* [-],

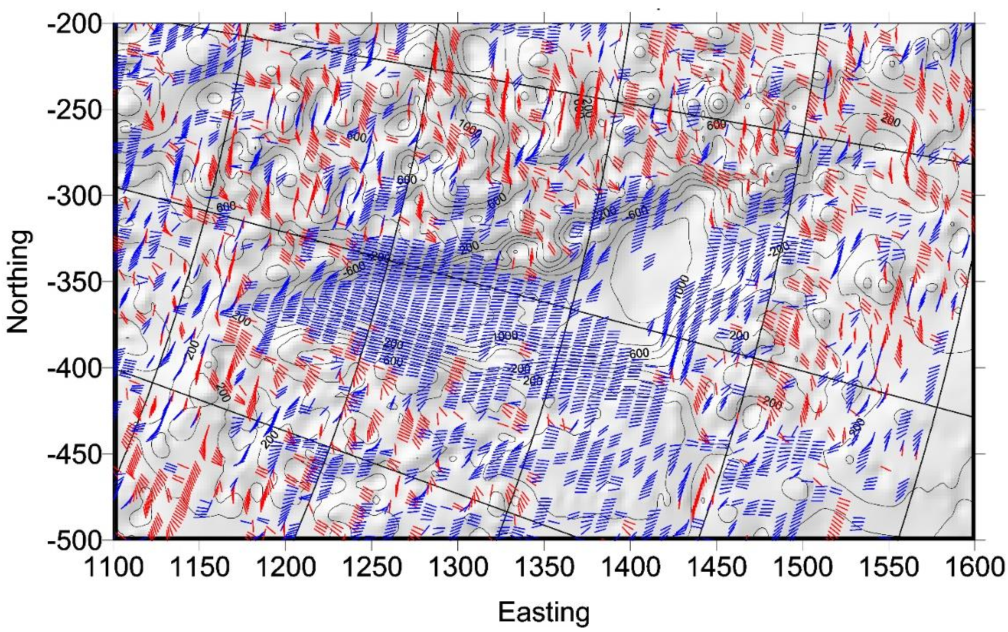

Fig. 10c and the strike angles θ [deg], $I < 0.3$, with the RET 14 model at LV, plus Bedmap 2. The circles in Fig. 10b show positions of two hypothetical subglacial volcanoes (Klokočník et al. 2016, 2017c); typical *vd* for any volcano. Note that in Figs. 10 a-c west is up / north on right

Other faults and similar geological features like Lake Baikal, the Dead Sea, Victoria Lake area, the Pacific Ocean with volcanoes on the ocean's bottom, east of Japan, Great Canyon, etc. show similar behaviour of the strike angles (and the gravity aspects in general) as LV here; some examples are in SM2.

4.1.3.2. OIL/GAS DEPOSITS – GENERAL COMMENT

The spatial distribution of the combed strike angles indicates oil/gas deposits, water, ground water, paleolakes and similar features – it was discovered by Klokočník and Kostelecký (2014) on the case of famous, large deposits of oil/gas in Ghawar (Saudi Arabia) and the Caspian Sea (Russia, Azerbaijan, Turkmenistan, and Iran). More localities were discussed in Klokočník et al. (2020a, 2021a), and they are the sources of majority of information for this part of our review.

Where the large TD (Target Deposits) concerning water, oil, gas, coal, hydrocarbons, sediments, or their various combinations or other very porous material (in a contrast to surroundings) are

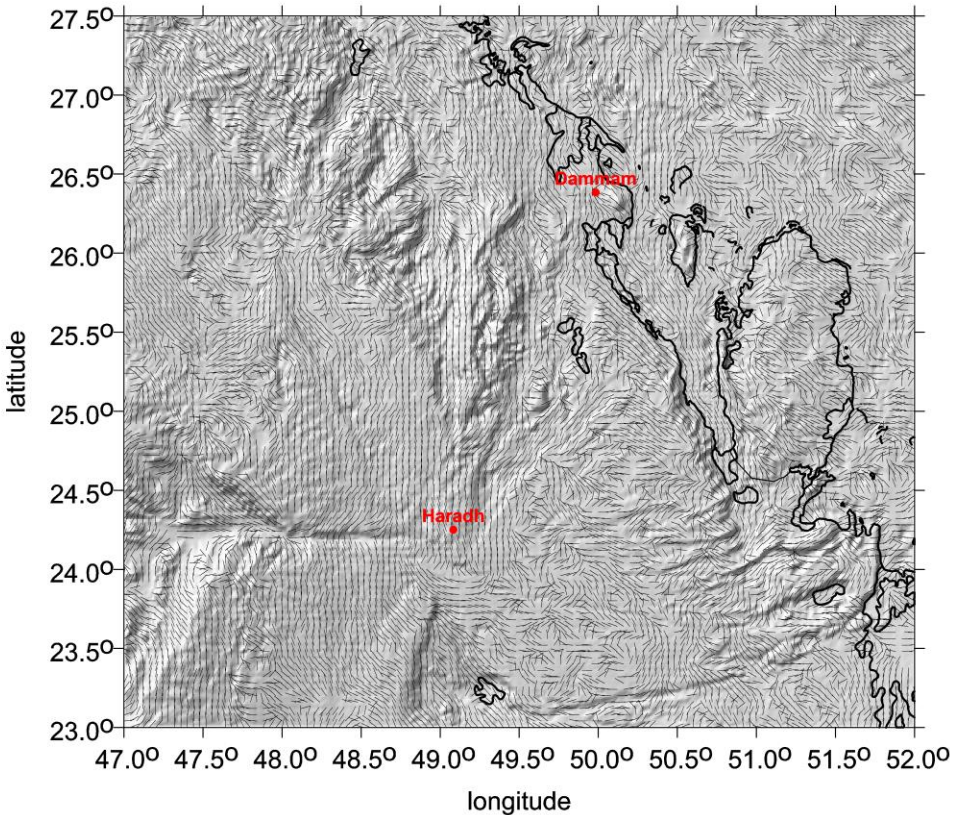

Fig. 11 The strike angles θ [deg], ($I<0.9$), for the Ghawar fields, Saudi Arabia (marked) and for a part of the Persian Gulf. ETOPO1 added [m].

known, there are ALWAYS seen (linearly) combed strike angles. Often the strike angles are combed not only there but also around, depending on many factors not yet well understood. But we can observe the combed θ also on other places without known oil/gas platforms; it *can be* due to not yet discovered TD.

The spatial distribution of the combed strike angles may indicate a new, cheap, accessible empirical geological/geophysical tool for recognition of potential hydrocarbon occurrences or water or both (but see the warning axioms in Sect. 2.1.) The method represents the first approximation for less accessible regions to decide to include or exclude them from more detailed investigations, thus potentially saving money before digging and drilling (Klokočník et al., 2020e, 2021c). However, recalling as a warning against too optimistic visions and repeating the axioms (Sect. 2.1): *(i)* the combed strike angles are *not* directly due TD or to gas, oil, coal, minerals, or water contained within the TD. *(ii)* the correlation (between the gravity aspects and locations of TD) does *not* imply causation.

We show examples for large, known deposits and mining sites at Ghawar, Gulf of Mexico, the Caspian Sea, Egypt/Israel, or hypothetical Doggerland (east-north of the Atlantic Ocean near Europe) and more in (Klokočník et al., 2021a). The ground water or paleolakes will be reminded by two samples of paleolakes in Sahara (in Egypt, see Sects. 4.1.3.7 and 4.1.3.8).

4.1.3.3. GHAWAR

Ghawar (in Saudi Arabia) is a large Hercynian basement horst, about 230 km long and 30 km wide, reactivated episodically. Ghawar is still the world's largest oil reserve (e.g., Afifi 2005, SM2:41-43). We present Figure 11 with the strike angles θ; they are combed in the NS-NE direction along the "TD line" ~200 km long (observe a change in the direction of alignment in its northern part). Interesting is that the combed θ continue N and SE out of that line. It corresponds to anticlinal structural evolution, where a part of the original source area for the natural gas palpably is located.

The orientation of strike angles around the Ghawar oil field is unusual. It is mainly the interface or contact zone of two large areas with different strike angles orientation. To the east of the Ghawar anticline we observe a rather chaotic arrangement. The roughly NS structure of Ghawar itself is made up of mostly parallel NS strike angles, such as usually correspond to compression conditions. These in turn led to formation of a long-developing horst and a long, narrow anticline that represents an oil trap. However, a compression zone with a similar strike angle orientation continues farther north, where we can expect similar pressure conditions but apparently degraded conditions for hydrocarbon deposition.

Of equal interest is the Arabian Basin, west of the Ghawar anticline. From a geotectonic point of view, it represents a quiet, almost uniformly arranged area,

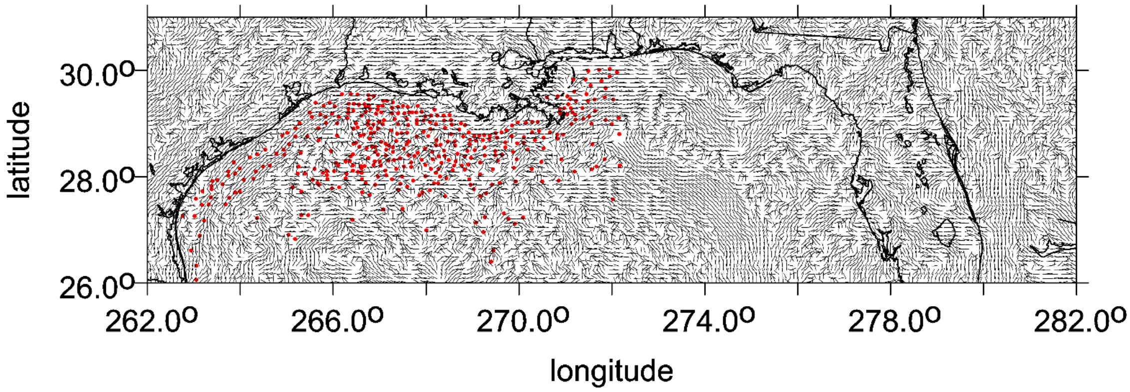

Fig. 12 The combed strikes angles (I<0.9) together with the dots for oil and gas platforms (according to ArcGIS data). More figures in SM2.

where hydrocarbon resource areas tend to be. These leak in tectonically fractured terrains into faulted and crushed zones. A closer look reveals a number of other features, such as similar quiet arrangement of the strike angles at the Khurais oil field, or the smaller east-west transverse structure south of Haradh that continues to probably tectonically based valley.

4.1.3.4. GULF OF MEXICO

The Gulf of Mexico Basin is a complex petroleum province covering parts of the sea shore. The source rocks have formed as Upper Jurassic limestones, Cretaceous marls and Palaeogene mudstones. These Jurassic sediments were quickly buried by almost 2 km thick Cretaceous sandstone and claystone. Some of the oil circulation structures may have been influenced by Chicxulub impact tectonics.

The well-known regional TD, oil/gas platforms, are superimposed over the combed θ (Fig. 12). We can see a good agreement. Note possible further promising TD in the Mexican Gulf in the direction to Florida, in a deeper sea (without the red dots in Fig. 12).

4.1.3.5. CASPIAN SEA

In Figures 13 a,b, we show the strike angles in the Caspian Sea together with positions of known hydrocarbon sources. Figure 13a shows a fair correlation between the places with the combed θ and the TD positions. See also the comments in Sects. 4.1.3.2. and 4.1.3.3.

We need, however, to warn the readers before a literal use of such comparisons (as for the correlation between the red dots and abscissae for θ about the alignment). The reason is that such maps as in Figure 13b can be not complete, with gaps, due to various reasons (missing or secret data), so a direct comparison between the strikes and the dots may be misleading. The same is valid for the Mediterranean Sea, now submerged Doggerland, for the Mexican Gulf, and many other places. But one can also speculate whether the combed strike angles zones, like the oval in Figure 13b, may signalize existence of further, not yet known deposits (recalling Sect. 2.1 and Klokočník et al., 2021a), or it is "something else".

4.1.3.6. *EAST/SOUTH OF THE MEDITERRANEAN SEA AND NORTH EGYPT*

Oil and gas deposits in this area are characteristic by huge thickness of mostly Mesozoic and Cenozoic sediments, by presence of salt diapers, several types of source and host rocks. The prominent tectonic feature is represented by the Dead Sea Rift, the Nile paleo-delta and Mediterranean micro-blocks, Sect. 4.1.1.2.

Figure 14 presents the combed strike angles in eastern/southern Mediterranean Sea together with positions of known hydrocarbon sources (the larges are Zohr and Leviathan). Again, a fair correlation between these two components exists. But we know that such maps can well be non-complete, as already mentioned, so a direct comparison between the strikes and the dots may be misleading (see above). Nevertheless, we confirm a fair correlation of the known TD sites and the reader can think about the other perspective locations.

4.1.3.7. EGYPT, WEST DESERT – GSS HYPOTHETICAL PALEOLAKE

When the river water or lake is filled with a sediment (sand, silt, clay), the density of the combined body of fluid (pool) and sediment becomes lower than before but still may contrast with respect to surrounding rocks (due to porosity contrast); this is what we detect (if the contrast is sufficiently large). Then the pre-existing body of water shows negative Δg and T_{zz} and specific values of the other gravity aspects (namely the strike angles θ which are there highly combed). This is observed, for example, at the Libyan-Egyptian border in the Great Sand Sea (GSS) – investigated in Klokočník et al. (2020e) or between town Kharga in the Western Desert of Egypt and Toshka near the river Nile (Klokočník et al., 2020f). Such signals may preserve for a long time, but endogenous and exogenous forces are transporting

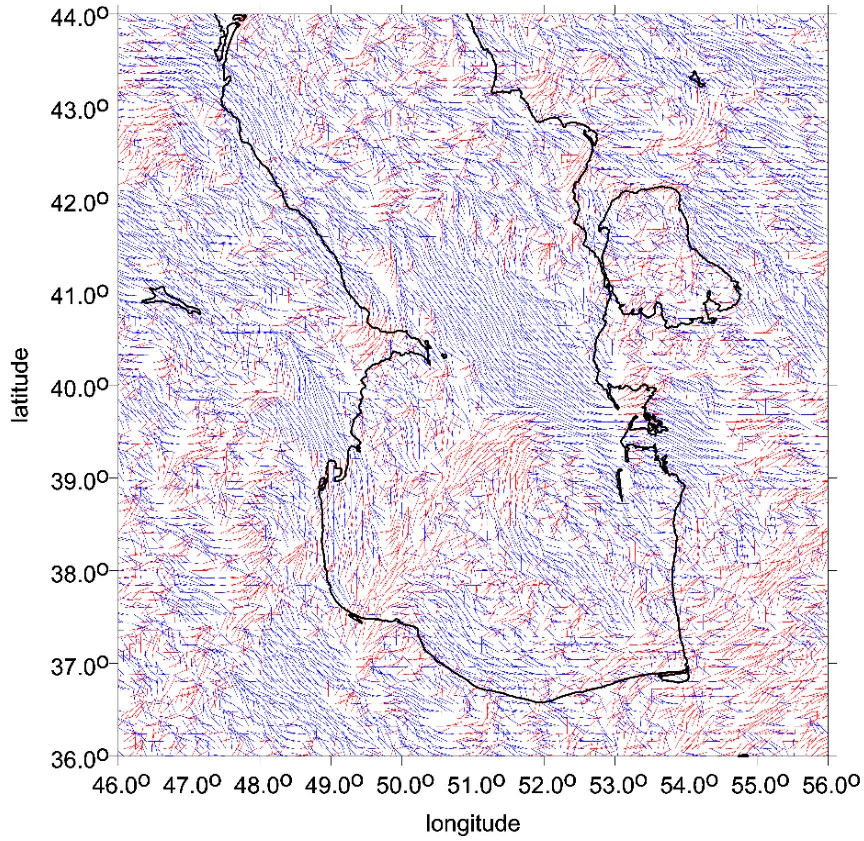

Fig. 13a The strike angles θ ($I<0.9$) for the Caspian Sea; red colour means direction to North and blue to South from East.

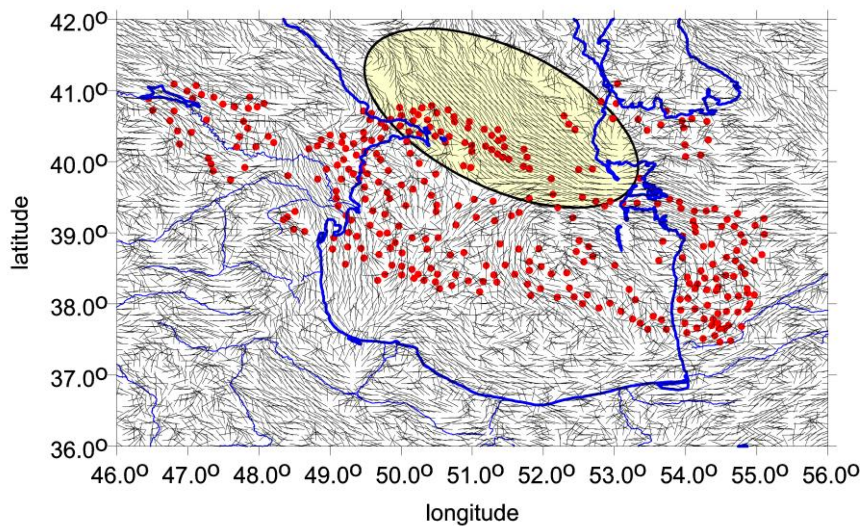

Fig. 13b The strike angles θ ($I<0.9$) for the southern part of the Caspian Sea; red dots for oil/gas platforms (Eppelbaum, 2023, priv. commun.; Kadirov et al., 2023). More figures in SM2.

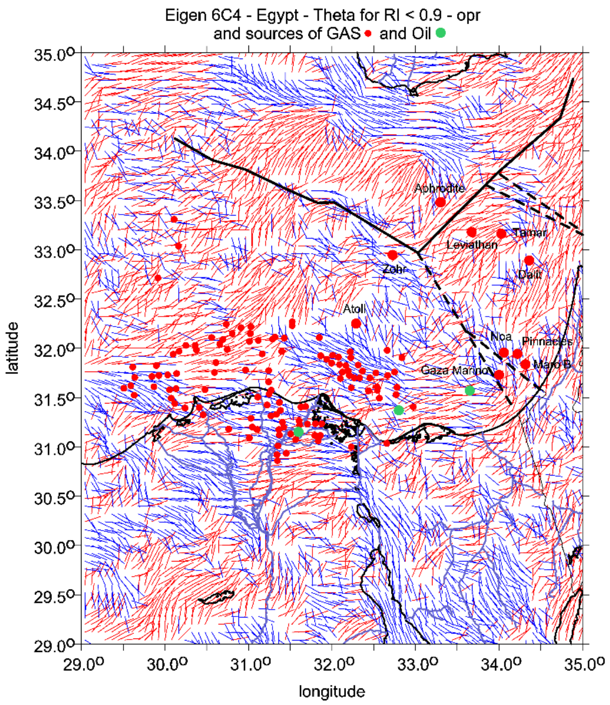

Fig. 14 The combed θ [deg] for the ratio I<0.9 with gas (red dots) and oil (green dots) platforms utilized in the delta of Nile and in the eastern/southern Mediterranean Sea.

masses and, in course of time, they inevitably transform the gravity signal.

We have tested several localities with hypothetical paleolakes in Sahara, namely the Lake MegaChad, Fazzan, Chotts, Tamanrasett river system or Kufrah Basin and confirmed their existence independently on the other investigators (Klokočník et al., 2017b). Moreover, we predicted one more hypothetical paleolake and paleorivers in Western Desert of Egypt (GSS), in the SN direction along the border of Egypt with Libya, (Klokočník et al., 2020e), running from the hills of Gilf Kebir (south) to the Siwa depression (north).

Figure 15a shows the strike angles and gravity disturbances in Egypt. The strike angles are perfectly combed in the zone of possible GSS paleolake(s), Western Desert. There might be several lakes from south to north, connected by rivers with waterfalls and rapids (Fig. 15b). The GSS hypothetical paleolake contained volume of cubic kilometres of clay and bound water. After desiccation, it was filled up with sediments and covered by a thick sand layer, up to 200 m thick (coming from north), as we know and can observe now. Often the dry out lakes (playa) have surrounding topography allowing existence of intermittent lakes and streams, that allow partial water filling during the occasional storms. While other localities support our conclusions by means of evident existence of archaeolocalities, here in the GSS along the border the past settlements if any may be hidden beneath those thick layers of sand (Klokočník et al., 2020e).

The profiles of present-day surface topography according to the ETOPO 1 and from Δg (from EIGEN 6C4) along the border (Fig. 10b) differ significantly. It indicates possible locations of the paleolake(s). The distance "zero" on the x-axis is at the Gilf Kebir hills on south and is counted to north roughly along the meridian (100 km ~ 1^0).

Also, the hidden hypothetical impact crater (the Silica region, latitude 25^015'–25^030'N, longitude ~25^030'E; not the Gilf Kebir crater' field!), the probable source of the famous ejecta known as "yellow glasses" (Libyan Desert Glass), can be located there (circular-like θ at the location).

4.1.3.8. EGYPT, KHARGA-TOSHKA

While the GSS in north-western Egypt (previous subsection) looks at first glance improbably as a (paleo)lake or a river system or a combination of both, the depression south of Kharga (Charga) looks as a very logical candidate (Figs. 16a,b). Archaeologists predicted that there was a lake. Its southern part is known for archaeolocalities (see references in Klokočník et al., 2020f).

There is evidently a great space for a lake/inner sea/river system some time ago when the Sahara was green; the lowland was filled, probably repeatedly, by water. Klokočník et al., (2020f) reconstructed the "Kharga-Toschka" paleolake and suggested its approximate mean extent using archaeological sites as external constraints (Fig. 16a).

The ETOPO1 topography and Δg of the area mainly between Kharga (town) and Toshka (depression, lakes) are shown in Figure 16a. A Middle Pleistocene (approx. 0.5 Ma) overflow of the Nile to the west through Wadi Toshka was proposed to account for the findings of lake remnants, fossil fish and paleochannel terminations at ~250 m to the south (Selima) and west (Bir Tarfawi, Bir Sahara) of this research area.

Figure 16b shows the strike angles for the same area. They are aligned, as expected, but it is not so intensive as in craters (probably the energy of the stresses on the local material was not so high). Figure 16b also indicates (due to their large-space NS alignment) a possibility that after the paleolake, in the direction N and NE of Kharga, a paleoriver continued, with possible waterfalls and cataracts. [This is only a speculation based on the gravity data].

In recent years, the local groundwater began to be exploited for agricultural reclamation projects, clearly visible on ©Google Earth, with circular fields watered by sprinklers using water pumped from the aquifer (e.g., El Oweinat project) or watermelon cultivation fields relying on near-surface water sources. The groundwater is not so deep and the paleolake and paleoriver system is well possible also from the gravity signal viewpoint.

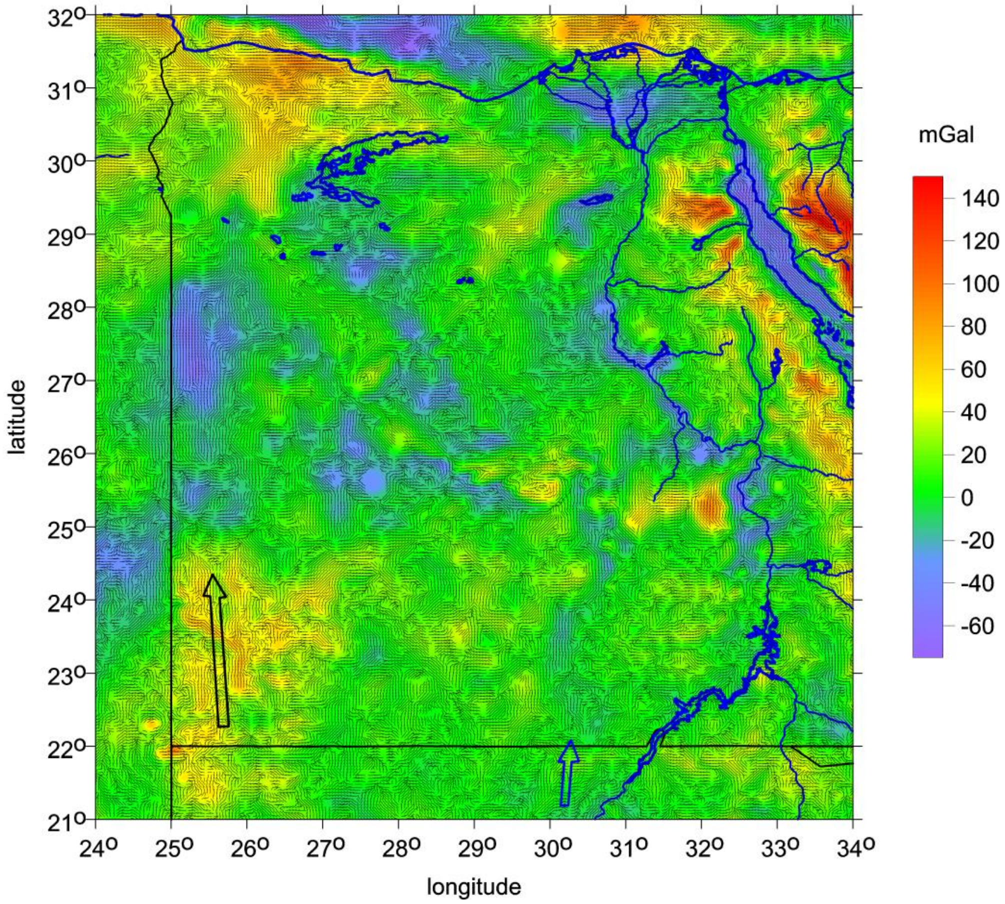

Fig. 15a The strike angles θ [deg] and Δg [mGal] for Egypt and hypothetical paleolakes in the Egyptian Western Desert, along the border with Libya, from the most southern point of Gilf Kebir hills to north to the Siwa depression-oasis, left black arrow, and between Toschka and Kharga (southern Egypt), blue arrow. Zooms and more figures are in S2. Note conspicuous negative Δg (blue) along the Libyan-Egyptian border where θ are highly aligned in the SN direction.

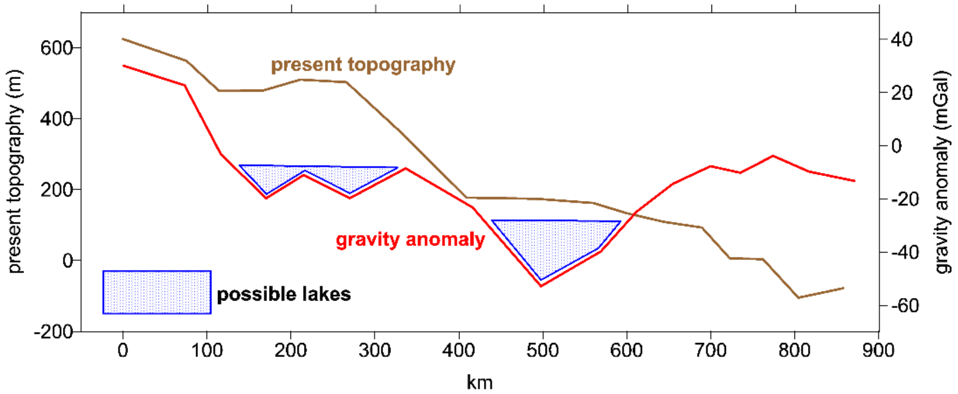

Fig. 15b The profiles of present surface topography from the global model ETOPO 1 and from gravity disturbances Δg derived from EIGEN 6C4 along the trace shown in Figure 15a (brown arrow) from south to north in western Egypt, indicating possible locations of the paleolake(s) including also the Eocene-Miocene impact crater, a putative source of LDG. The distance "zero" on the *x*-axis is at Gilf Kebir and is counted to north roughly along the meridian. Roughly it holds that 100 km = 1^0

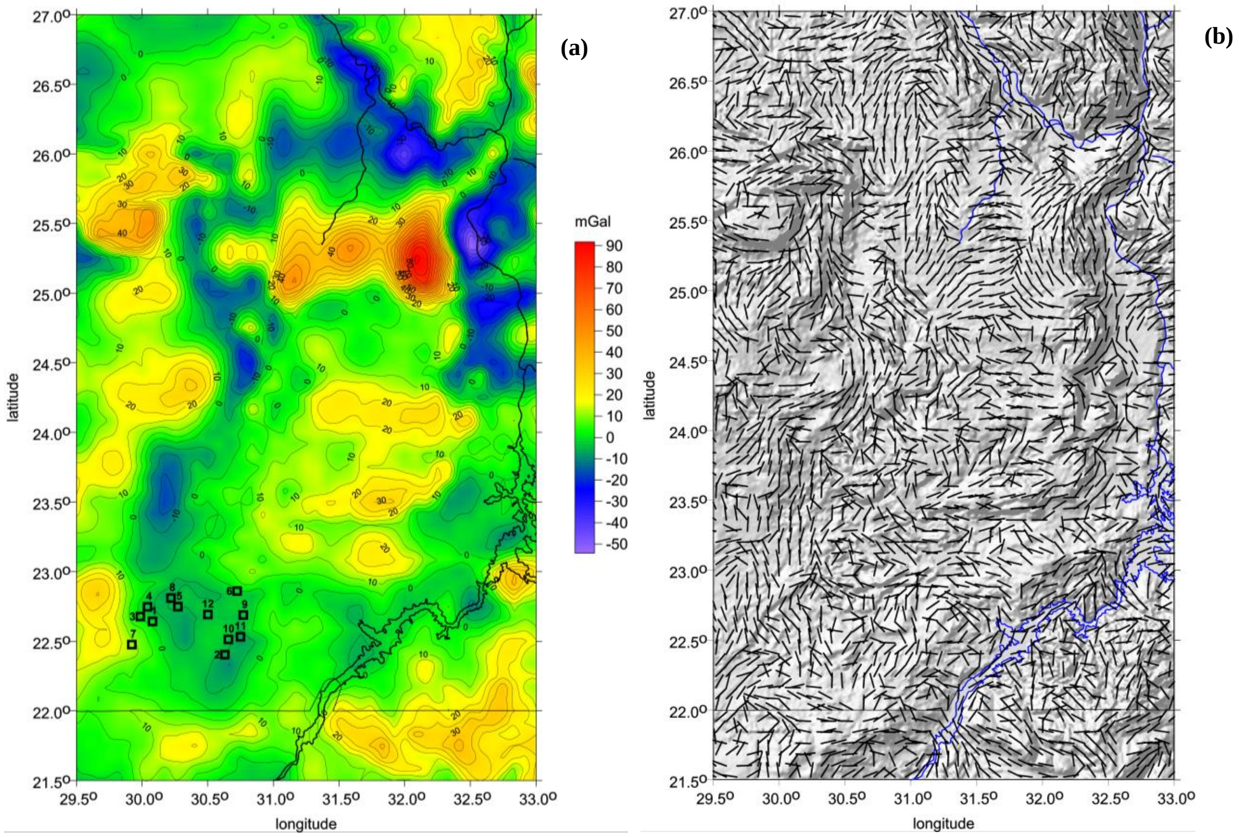

Figs. 16 a,b **(a)** The position and extent of the huge hypothetical paleolake(s) between Kharga and Toshka (town) and Toshka (depression at the river Nile), Southern Egypt, versus Δg [mGal] (EIGEN 6C4). The squares show archaeological sites; **(b)** the strike angles θ [deg]; ETOPO 1 topography as 3D shadows added. The river Nile in black or blue colour.

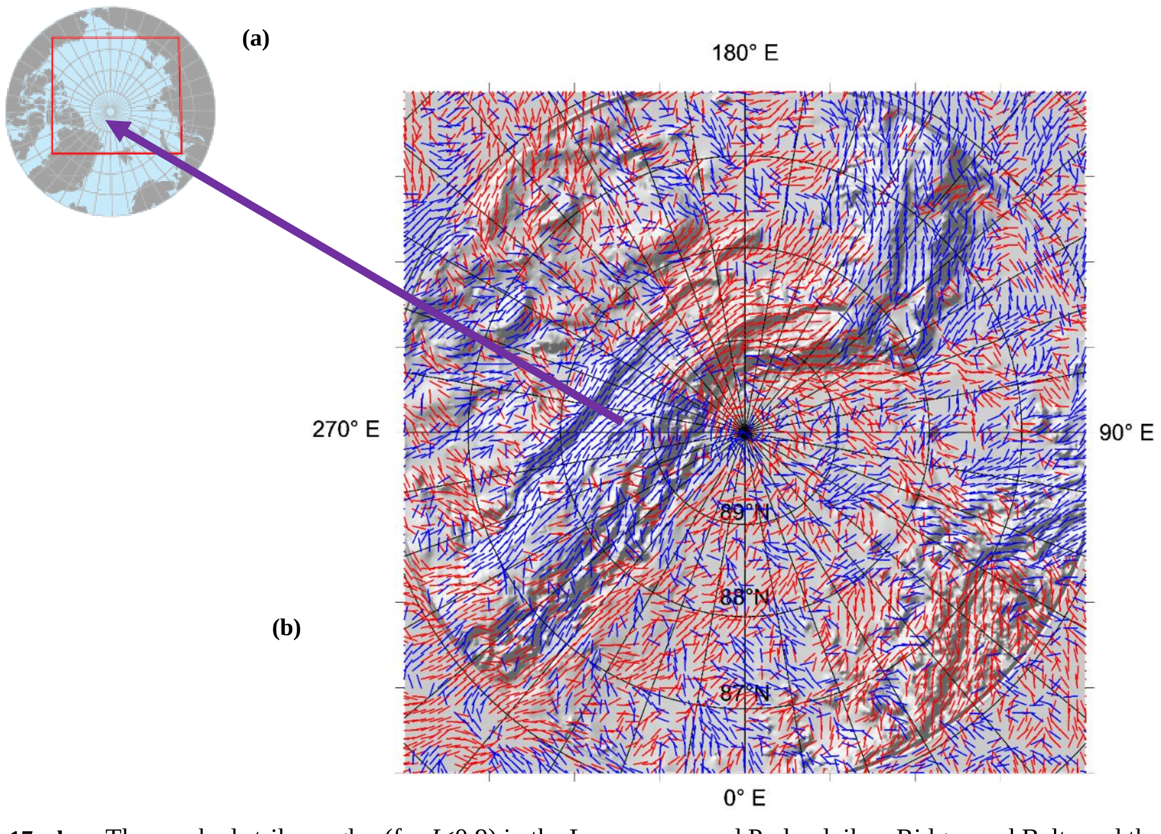

Figs. 17 a,b The combed strike angles (for I<0.9) in the Lomonosov and Podvodnikov Ridges and Belts and the Arctic Ocean around; the ocean topography from ETOPO1 [m].

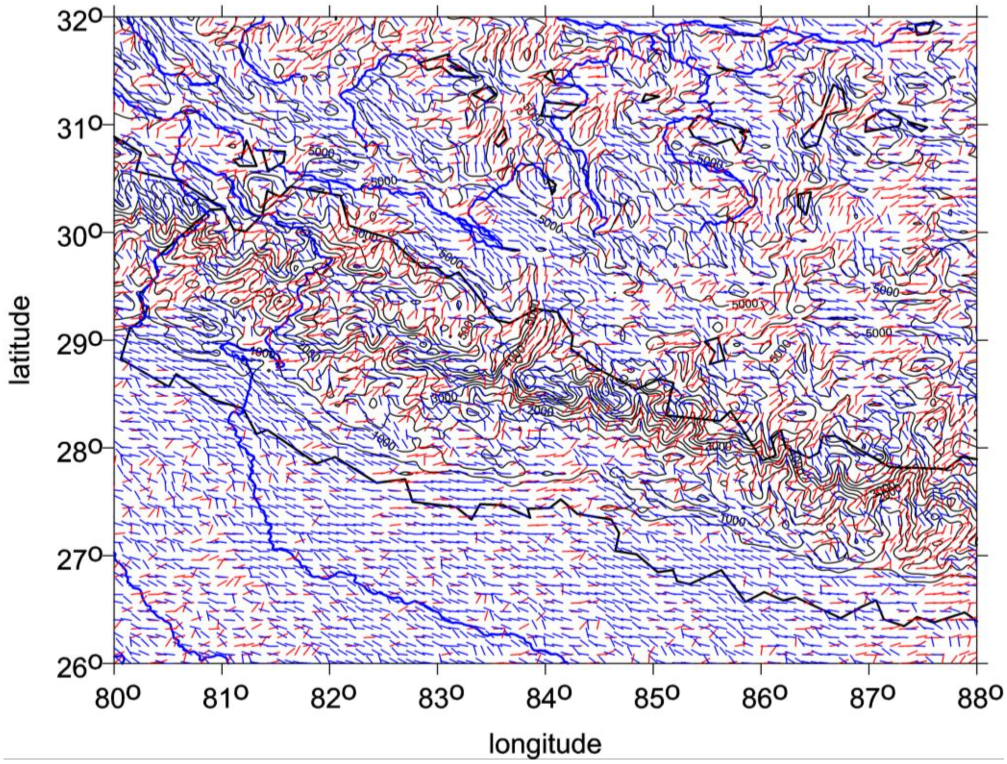

Fig. 18 The strike angles (for I<0.9) in the Himalaya and its neighbouring areas; with contours of topography from ETOPO1 [m].

4.1.4. OTHER GEOLOGICAL FEATURES

4.1.4.1. LOMONOSOV RIDGE, THE ARCTIC OCEAN

The Lomonosov Ridge (LR) is one of the most prominent topographic features in the Arctic Ocean. The Arctic Ocean (AO) is rich in hydrocarbon resources, including the LR. We investigated AO with the gravity aspects to detect zones on land and in the sea with conditions favourable for hydrocarbon occurrences (Klokočník et al., 2025b). We found that LR fulfils the requirements for possible hydrocarbons bearing sediments along its both sides; we observed highly combed strike angles along the long axis of LR (Fig. 17b). The strike angles indicate a great potential for petroliferous layers and not only in LR. Huge West Siberian basin and Yamal peninsula nearby, with known and large oil/gas resources, were used as a testbed demonstrating that our method works well.

Our results can also be used for speculations about further untapped places in the AO with prospective hydrocarbon resources. The exploring of oil and gas and a future production in the Arctic would be financially very demanding; we can help to minimize fails, reduce costs and environmental damages. There are conflicting aspects of the hydrocarbon drilling in the AO such as tension between Arctic environmental protection and offshore oil and gas development. The best would be not to drill there at all, because there are still sufficient, less risky, and cheaper sources on land.

4.1.4.2. HIMALAYA

The strike angles have been used in morphological studies of processes and events being under way of collisional orogeny between the Indian and Asian lithospheric plates in the Nepal Himalaya (Kostelecký et al., 2024). The leading regional driving forces determining directions of θ are thrust faulting stress forces approximately to the north and its subduction under southern part of the Asian continental plate. The density and arrangement of the mass in interior of the subducted plate operating in the zone of collisional orogeny is dominated by compression tectonic regimes controlled above all by the course of slab pull. Figure 18 presents the strike lines of θ (I<0.9). A series of the relevant figures is in SM2: 118-127.

4.2. NOTES ABOUT THE MOON AND MARS

We only shortly outline our studies of the Moon and Mars via the gravity aspects. Many figures are in S3 and S4. We work with the gravity model GRGM1200A (Lemoine et al., 2014) for the Moon and the JPL JGMRO_120 F (Konopliv et al., 2020) for Mars (Sect.2.3) with the ground resolutions 10 km and 130 km, respectively.

Kletetschka et al., (2022) suggested a new hypothesis how the oxygen ions from the Earth's atmosphere can be transferred via the magnetosphere to the Moon to create ground water. Recently, Klokočník et al (2025c) contributed to search for the ground water at the southern pole of the Moon for the forthcoming permanent lunar human missions. Klokočník et al. (2022a) investigated how the gravity signal in terms of the gravity aspects look like for the impact craters, mascons (mass concentrations) or maria (S3). Our *Atlas of the Gravity and Magnetic Fields of the Moon* (Klokočník et al., 2022c) presents all the gravity aspects, LOLA topography and magnetic intensities for the Moon, divided into segments.

The gravity aspects were used to study various features (volcanoes, trenches, craters, hypothetical Northern Martian Paleoocean) on Mars (Klokočník et al., 2023b). The strike angles, namely in the paleoocean, create very large areas with highly combed signal. They look like the known, large oil/gas deposits on the Earth; thus we speculate about possibility of the hydrocarbon occurrences on Mars (Klokočník et al., 2023c).

5. CONCLUSION

All the gravity/gravitational aspects – the gravity disturbances (anomalies) Δg, Marussi tensor $\mathbf{\Gamma}$, the gravity invariants I_1 and I_2 and their specific ratio I, the virtual deformations *vd* and the gravity strike angles θ – (for the formulae see SM1), used together, yield more comprehensive, far more complete information (but more complicated to compute) about the ground density anomalies comparing with the traditional approach when only locally measured gravity anomalies (sometimes amended by the radial component of the Marussi tensor or the full Marussi tensor) are at disposal.

The gravity aspects in our approach are global-based values, non-linear combinations of the harmonic geopotential coefficients (Stokes parameters) C_{lm}, S_{lm} of the static global gravity/gravitational field models of the studied celestial bodies. With the gravitational aspects, derived from the present-day gravity models of the Earth, the Moon, and Mars (the best what is available now for this purpose), already sufficiently precise and with a reasonable ground resolution, we can begin with the actual “gravitational tomography”.

The combed strike angles (the strike angles aligned into one direction along or ordered around the feature in question) were proved to be very efficient for various geological, geophysical and other interpretations, provided that not only the gravity data are available.

Craters: The impact energy is imprinted into the gravity aspects. The strike angles are combed into circular halos around the craters, along the rims. The release of the energy of the impactor triggers the stress in the rock along the cleavage planes. Traces after the energy can be detected by the combed strike angles. Rivers, canyons, faults, groundwater or ice, permafrost (on the Earth), regolith (on the Moon), paleo-lakes, hydrocarbon occurrences, and sedimentary layers: they are typical of linearly combed strike angles. Such an alignment is not only a reaction to a higher porosity/lower density, but also an answer to stress, a force connected with genesis and evolution of such features.

The impact craters as well as uncertain (hypothetical) and impact-related phenomena have been studied. Chicxulub (Sect. 4.1.2.1.) exhibits combed strike angles to halos around the subsurface (land) part of the crater. Chicxulub can be a double crater. The strike angles at Vredefort show halos (two conspicuous plus one fragmented), a central peak, and probably one additional smaller crater, in the SE direction of the main crater (Sect. 4.1.2.2.). Ries structure (and even its small companion Steinheim) is identified by the combed strike angles. In good agreement with findings by geologists, the strike angles predict the direction of the falling impactor from SW (Sect. 4.1.2.3).

Sudbury basin, rich in economical minerals, also depicts the expected effects (Sect. 4.1.2.4). Popigai structure appears as a multiple crater, with the impactor direction from SE/NW or NW/SE (Sect. 4.1.2.5). Saginaw Bay event can well be a consequence of an impact (on ice), without any big crater, because the explosion may take place in the atmosphere and/or subsequent deglaciation removed smaller original craters on the ice cover. Our further findings concern the Hiawatha crater in Greenland, Kotuykanskaya in Siberia near Popigai, Badain in China, Burckle in the Indian ocean or Tunguska.

Subglacial volcanoes, lakes and impact craters have been discovered or their discovery independently confirmed. Near Lake Vostok, east Antarctica, we discovered two possible subglacial volcanoes and three lakes, and in Wilkes Land, our results support the hypothesis about a huge impact basin with a mascon (!, Sect. 4.1.3.1).

The areas with a lower density (higher porosity) material (than in surrounds) have been studied. The strike angles in the zones with low density background are typically highly combed and create large “plates” with specific orientations. We speak about paleolake/river systems, oil/gas deposits or possible ground water reservoirs, already known or prospective. *Hydrocarbon deposits* in Ghawar, the Persian Gulf, the Gulf of Mexico, west/south of Chicxulub, the Caspian Sea, north Egypt, and west Israel (in the sea), and many more places have been tested (Sects. 4.1.3.3 – 4.1.3.6). Several known paleolakes on the Sahara were confirmed (Lake MegaChad, MegaFazzan, Chotts, Kufrah Basin or Tamanraset) and two more were suggested. These should be in west Egypt (Sect. 4.1.3.7) and in south Egypt (Sect. 4.1.3.8).

The spatial distribution of the combed strike angles may indicate a new cheap and accessible empirical remote sensing geophysical tool for recognition of some potential hydrocarbon occurrences or water or both. The method put forward “a zero approximation” for less accessible regions to decide to include or exclude them from more detailed subsequent investigation, thus potentially saving money. The strike angles can be useful before drilling, as a diagnostic tool, in combination with traditional terrestrial methods, various mineralogical-petrological analyses, and others.

The gravity aspects can be applied universally to all terrestrial planets – of course accounting for their diverse geology, and provided that their gravity field is already known with sufficient reliability and ground resolution (now it is true for the Earth, the Moon, and Mars).

ACKNOWLEDGMENTS

This work was supported by the projects RVO 67985815 and RVO 67985831 (Czech Academy of Sciences, Czech Republic).

DECLARATION OF COMPETING INTEREST

The authors declare that they have no competing financial interests or personal relationships that could have appeared to influence the work reported in this paper.

DATA AVAILABILITY

The input data – the harmonic geopotential coefficients of the gravity field models and topography models – are publicly available; data to our figures (surfer program) and our figures with high resolution (.png files) can be received from Jan Kostelecký on a request.

AUTHOR CONTRIBUTIONS

Figures were plotted using *surfer* software by Jan Kostelecký.
Data curation: mainly Aleš Bezděk.
Formal analysis, Methodology, Validation, Writing – review & editing: all authors;
Project Administration, Resources: Jaroslav Klokočník, Aleš Bezděk
Software, Visualization: Aleš Bezděk, Jan Kostelecký
Writing – original draft, Supervision: Jaroslav Klokočník, Václav Cílek.

APPENDIX. SUPPLEMENTARY DATA

https://www.asu.cas.cz/~jklokocn/Strikes_25_Supplements/

REFERENCES

Afifi, A.M.: 2005, Ghawar: The Anatomy of the World's Largest Oil Field. Search and Discovery, AAPG/Datapages, Inc., #20026.

Alvarez, L., Alvarez, W., Asaro, F. and Michel, H.V.: 1980, Extraterrestrial cause for the cretaceous-Tertiary extinction. Science, 208, 4408, 1095–1108. DOI: 10.1126/science.208.4448.1095

Amante, C. and Eakins, B.W.: 2009, ETOPO1 1 arc-minute global relief model: procedures, data sources and analysis. NOAA Techn. Memo. NESDIS NGDC 24 (National Geophysical Data Center). DOI: 10.7289/V5C8276M

Beiki, M. and Pedersen, L.B.: 2010, Eigenvector analysis of gravity gradient tensor to locate geologic bodies. Geophysics, 75, 137–149. DOI: 10.1190/1.3484098

Boslough, M., Nicoll, K., Holliday, V., Daulton, T.L., Meltzer, D., Pinter, N., Scott, A.C., Surovell, T., Claeys, P., Gill, J., Paquay, F., Marlon, J., Bartlein, P., Whitlock, C., Grayson, D. and Jull, A.J.T.: 2012, Arguments and evidence against a younger dryas impact event. Geophys. Monogr. Ser., 198, 13–26. DOI: 10.1029/2012GM001209

Bucha, B. and Janák, J.: 2013, A MATLAB-based graphical user interface program for computing functionals of the geopotential up to ultra-high degrees and orders. Comput. Geosci.**,** 56, 186–196. DOI: 10.1016/j.cageo.2013.03.012

Buchner, E., Volker, Sach, V.J. and Schmieder, M.: 2022, Event- and biostratigraphic evidence for two independent Ries and Steinheim asteroid impacts in the Middle Miocene. Sci. Rep., 12, 1. DOI: 10.1038/s41598-022-21409-8

Castaldo, R., Fedi, M. and Florio, G.: 2014, Multiscale estimation of excess mass from gravity data. Geophys. J. Int.**,** 197, 1387–1398. DOI: 10.1093/gji/ggu082

Chlupáč, I., Brzobohatý, R., Kovanda, J. and Stráník, Z.: 2002, Geological history of the Czech Republic. Academia Praha, (in Czech).

Davias, M.E. and Harris, T.H.S.: 2015, A tale of two craters: Coriolis-aware trajectory analysis correlates two pleistocene impact strewn fields and gives Michigan a thumb. Geological Society of America Abstracts with Programs, 47, 5, 4.

Davias, M. and Harris, T.H.S.: 2022, Postulating an unconventional location for the missing mid-Pleistocene transition impact: Repaving North America with a cavitated regolith blanket while dispatching Australasian tektites and giving Michigan a thumb. In: Foulger, G.R., Hamilton, L.C., Jurdy, D.M., Stein, C.A., Howard, K.A. and Stein, S., eds., The Footsteps of Warren B. Hamilton: New Ideas in Earth Science. DOI: 10.1130/2021.2553(24)

Donofrio, R.R.: 1998, North American impact structures hold giant field potential. Oil Gas J., 96, 69–83.

Ebbing, J. et al.: 2018, Earth tectonics as seen by GOCE - Enhanced satellite gravity gradient imaging. Sci. Rep., 8, 16356. DOI: 10.1038/s41598-018-34733-9

Eppelbaum, L.: 2017, Satellite gravimetry (´Big Data´), - a powerful tool for regional tectonic examination and reconstructions. In: Veress, B. and Szigethy, J. (Eds.), Horizons in Earth Science Research, 17, Chapter 4. Nova Sci. Publ.

Eppelbaum, L.V. and Katz, Y.I.: 2017, A new regard on the tectonic map of the Arabian-African region inferred from the satellite gravity analysis. Acta Geophys., 65, 607–626. DOI: 10.1007/s11600-017-0057-2

Eppelbaum, L., Katz, Y., Klokočník, J., Kostelecký, J., Ben-Avraham, Z. and Zheludev, V.: 2018, Tectonic insights into the Arabian-African region inferred from a comprehensive examination of satellite gravity big data. Glob. Planet. Change, 171, 65–87. DOI: 10.1016/j.gloplacha.2017.10.011

Eppelbaum, L.V., Katz, Y.I. and Ben-Avraham, Z.: 2024, The reasons for enormous accumulation of the geodynamic tension in Eastern Turkey: a multidisciplinary study. Geology Geophys. Earth Sci., 2, 2, 1–28. DOI: 10.58396/gges020202

FitzGerald, D. and Holstein, H.: 2014, Structural geology observations derived from full tensor gravity gradiometry over rift systems. Conference, SEG Tech. Program Expand. Abstr., 1324–1328. DOI: 10.1190/segam2014-0964.1

Firestone, R.B. and Topping, W.: 2001, Terrestrial evidence of a nuclear catastrophe in Paleoindian times. Mammoth Trumpet, 16, 2, 9–16.

Firestone, R.B., West, A., Kennett, J.P., Becker, L., Bunch, T.E., Revay, Z.S., Schultz, P.H., Belgya, T. et al.: 2007, Evidence for an extraterrestrial impact 12,900 years ago that contributed to the megafaunal extinctions and the Younger Dryas cooling. Proc. Natl. Acad. Sci., USA, 104, 16016–16021. DOI: 10.1073/pnas.0706977104

Foulger, G.R.: 2010, Plates vs Plumes-A Geological Controversy. Wiley-Blackwell, xi+328. DOI: 10.1002/9781444324860

Förste, Ch., Bruinsma, S., Abrykosov, O., Lemoine J-M. et al.: 2014, EIGEN 6C4-The latest combined global gravity field model including GOCE data up to degree and order 2190 of GFZ Potsdam and GRGS Toulouse. 5th GOCE User Workshop, Paris 25–28 Nov. 2014.

Fretwell, P., Pritchard, H., Vaughan, D. et al.: 2013, Bedmap2: improved ice bed, surface and thickness datasets for Antarctica. Cryosphere, 7, 375–393. DOI: 10.5194/tc-7-375

Goderis, S. et al.: 2021, Globally distributed iridium layer preserved within the Chicxulub impact structure. Sci. Adv., 7, 9. DOI: 10.1126/sciadv.abe3647

Goossens, S. and Smith, D.E.: 2023, Gravity degree–depth relationship using point mass spherical. Geophys. J. Int., 233, 1878–1889. DOI: 10.1093/gji/ggad036

Grieve, R.A.F.: 2005, Economic natural resource deposits at terrestrial imapct structures. Geolog. Soc. London, Spec. Publs., 248, 1, 1–29. DOI: 10.1144/GSL.SP.2005.248.01.01

Heidbach, O., Rajabi, M., Cui, X., Fuchs, K., Müller, B., Reinecker, J., Reiter, K., Tingay, M., Wenzel, F., Xie, F., Ziegler, O.M., Zoback, M.L. and Zoback, M.: 2018, The World Stress Map database release 2016: Crustal stress pattern across scales. Tectonophysics, 744, 484–498. DOI: 10.1016/j.tecto.2018.07.007

Hildebrand, A.R. and Boynton, W.V.: 1990, Proximal Cretaceous-Tertiary boundary impact deposits in the Caribbean. *Science*, 248, 843–847. DOI: 10.1126/science.248.4957.843

Hildebrand, A.R. et al.: 1995, Size and structure of the Chicxulub crater revealed by horizontal gravity gradients and cenotes. Nature, 376, 6539, 415–417. DOI: 10.1038/376415a0.2013

Hirt, C. and Rexer, M.: 2015, Earth2014: 1 arc-min shape, topography, bedrock and ice-sheet models – Available as gridded data and degree-10,800 spherical harmonics. Int. J. Appl. Earth Obs. Geoinf., 39, 103–112. DOI: 10.1016/j.jag.2015.03.001

Hirt, Ch., Rexer, M., Scheinert, M., Pail, R., Claessens, S. and Holmes, S.: 2016, A new degree-2190 (10 km resolution) gravity field model for Antarctica developed from GRACE, GOCE and Bedmap 2 data. J. Geod., 90, 105–127. DOI: 10.1007/s00190-015-0857-6

James, S., Chandran, S., Santosh, M., Pradeepkumar, A.P., Praveen, M.N. and Sajinkumar, K.S.: 2002, Meteorite impact craters as hotspots for mineral resources and energy fuels: A global review. Energy Geosci., 3, 2, 136–146. DOI: 10.1016/j.engeos.2021.12.006

Kadirov, F.A., Klokočník, J., Eppelbaum, L.V., Kostelecký, J. and Bezděk, A.: 2023, Integration of the Bouguer gravity data with the satellite gravity transformations in the Caspian region and its tectonic-geodynamic significance. Conference Modern Ways for Searching Hydrocarbon Deposits, Baku, Azerbaijan (28-31 May).

Karimi, K., Kletetschka, G., Mizera, J., Meier, V., Strunga, V. et al.: 2023, Formation of Australasian tektites from gravity and magnetic indicators. Sci. Rep., 13, 12868. DOI: 10.1038/s41598-023-40177-7

Kalvoda, J., Klokočník, J., Kostelecký, J. and Bezděk, A.: 2013, Mass distribution of Earth landforms determined by aspects of the geopotential as computed from the global gravity field model EGM 2008. Acta Univ. Carol. Geogr., 48, 17–25.

Khazanovitch-Wulff, K.M., Mikheeva, V. and Kuznetsov, V.F.: 2013, Structural elements of some astroblemes indicating direction of cosmic body trajectories. New Concepts in Global Tectonics, 1, 3, 11–18.

Kletetschka, G. et al.: 2019, New implications for Tunguska explosion based on magnetic, dendrological, and lacustrine records. 82th Annual Meeting of the Meteoritical Society, Sapporo, Japan.

Kletetschka, G., Klokočník, J., Hasson, N., Kostelecký, J., Bezděk, A. and Karimi, K.: 2022, Distribution of water phase near the poles of the Moon from gravity aspects. Sci. Reps., 12, 1, 4501. DOI: 10.1038/s41598-022-08305-x

Klokočník, J. and Kostelecký, J.: 2014, Gravity signal at Ghawar, Saudi Arabia, from the global gravitational field model EGM 2008 and similarities around. Arab. J. Geosci., 8, 3515–3522. DOI: 10.1007/s12517-014-1491-y

Klokočník, J., Kostelecký, J., Pešek, I., Novák, P., Wagner, C.A. and Sebera, J.: 2010, Candidates for multiple impact craters? Popigai and Chicxulub as seen by the global high resolution Gravitational Field Model EGM08. EGU Solid Earth, 1, 71–83. DOI: 10.5194/se-1-71-2010

Klokočník, J., Kalvoda, J., Kostelecký, J., Eppelbau,m, L.V. and Bezděk, A.: 2014, Gravity disturbances, Marussi tensor, invariants and other functions of the geopotential represented by EGM 2008. Earth Sci. Res., 2, 3, 88–101. DOI: 10.18005/JESR0203003

Klokočník J., Kostelecký J. and Bezděk, A.: 2016, On feasibility to detect volcanoes Hidden under of Antarctica via their “Gravitational Signal". Annals Geoph., 59, 5, S053. DOI: 10.4401/ag-7102

Klokočník, J., Kostelecký, J. and Bezděk A.: 2017a, Gravitational Atlas of Antarctica. Springer International Publishing, 113 pp.

Klokočník, J., Kostelecký, J., Cílek, V., Bezděk, A. and Pešek, I.: 2017b, A support for the existence of paleolakes and paleorivers buried under Saharan sand by means of “gravitational signal” from EIGEN 6C4. Arab. J. Geosci., 10, 199. DOI: 10.1007/s12517-017-2962-8

Klokočník, J., Kostelecký, J., Bezděk, A. and Pešek, I.: 2017c, Candidates for volcanoes under the ice of Antarctica detected by their gravito-topographic signal. Ann. Geoph., 60, 6, S0661. DOI: 10.441/ag-7427

Klokočník, J., Kostelecký, J., Cílek, V, Bezděk, A. and Pešek, I.: 2018a, Gravito-topographic signal of the Lake Vostok area, Antarctica, with the most recent data. Polar Sci., 17, 59–74. DOI: 10.1016/j.polar.2018.05.002

Klokočník, J., Kostelecký, J. and Bezděk, A.: 2018b, On the detection of the Wilkes Land impact crater. Earth Planets Space, 70, 135. DOI: 10.1186/s40623-018-0904-7

Klokočník, J., Kostelecký, J. and Bezděk, A.: 2019, The putative Saginaw impact structure, Michigan, Lake Huron, in the light of gravity aspects derived from recent EIGEN 6C4 gravity field model. J. Great Lakes Res., 45, 12–20. DOI: 10.1016/j.jglr.2018.11.013

Klokočník, J., Kostelecký, J., Cílek, V. and Bezděk, A.: 2020a, Subglacial and underground structures detected from recent gravito-topography data. Cambridge SP.

Klokočník, J., Kostelecký, J., Bezděk, A. and Kletetschka, G.: 2020b, Gravity strike angles: a modern approach and tool to estimate the direction of impactors of meteoritic craters. Planet. Space Sci., 194, 105113. DOI: 10.1016/j.pss.2020.105113

Klokočník, J., Kostelecký, J., Bezděk, A., Cílek, V., Kletetschka G. and Staňková, H.: 2020c, Support for two subglacial impact craters in northwest Greenland from Earth gravity model EIGEN 6C4 and other data. Tectonophysics, 780, 228396. DOI: 10.1016/j.tecto.2020.228396

Klokočník, J., Kostelecký, J., Bezděk, A., Kletetschka, G. and Staňková, H.: 2020d, A 200 km suspected impact crater Kotuykanskaya near Popigai, Siberia, in the light of new gravity aspects from EIGEN 6C4, and other data. Sci. Rep., 10, 6093. DOI: 10.1038/s41598-020-62998-6

Klokočník, J., Kostelecký, J., Varadzinová, L., Bezděk, A. and Kletetschka, G.A.: 2020e, Gravity search for oil and gas and groundwater in Egypt using the strike angles derived from EIGEN 6C4. Appl. Sci., 10. DOI: 10.3390/app10248950

Klokočník, J., Cílek, V., Kostelecký, J. and Bezděk, A.: 2020f, Gravity aspects from recent Earth gravity model EIGEN 6C4 for geoscience and archaeology in Sahara, Egypt. J. Afr. Earth Sci., 168, 103867. DOI: 10.1016/j.jafrearsci.2020.103867

Klokočník, J., Kostelecký, J. and Bezděk, A.: 2020g, Response to comment by Schaetzl et al. (2019) on “The putative Saginaw impact structure, Michigan, Lake Huron, in the light of gravity aspects derived from recent EIGEN 6C4 gravity field model”. J. Great Lakes Res., 45, 1007–1009. DOI: 10.1016/j.jglr.2019.07.004

Klokočník, J., Kostelecký, J., Bezděk, A. and Cílek, V.: 2021a, The spatial distribution of the strike angles derived from EIGEN 6C4 gravity model - a new possibility for oil and gas exploration. Int. J. Oil Gas Coal Technol., 28, 3, 306–332. DOI: 10.1504/IJOGCT.2021.118651

Klokočník, J., Kostelecký J., Bezděk, A. and Kletetschka, G.: 2021b, Artefacts in gravity field modelling. Acta Geodyn. Geomater., 18, 4, 511–524. DOI: 10.13168/AGG.2021.0036

Klokočník, J., Kostelecký, J., Cílek, V., Kletetschka, G. and Bezděk, A.: 2022a, Gravity aspects from recent gravity field model GRGM1200A of the Moon and analysis of magnetic data. Icarus, 384, 115086. DOI: 10.1016/j.icarus.2022.115086

Klokočník, J., Bezděk, A. and Kostelecky, J.: 2022b, Gravity field aspects for identification of cosmic impact on Earth. In: Foulger, G.R., Hamilton, L.C., Jurdy, D.M., Stein, C.A., Howard, K.A. and Stein, S., eds., The Footsteps of Warren B. Hamilton: New Ideas in Earth Science. Geolog. Geol. Soc. Am., 251–260. DOI: 10.1130/2021.2553(21)

Klokočník, J., Kostelecký, J., Cílek, V., Bezděk, A. and Kletetschka, G.: 2022c, Atlas of the Gravity and Magnetic Fields of the Moon. Springer, 263 pp. DOI: 10.1007/978-3-031-08867-4_2

Klokočník, J. Kostelecký, J. and Bezděk, A.: 2023a, Gravity strike angles as admirable tool to study gravity fields of planets. Congress IUGG Berlin, Symp. G06a Monitoring and Understanding the Dynamic Earth Study Gravity Fields of Planets.

Klokočník, J. Kletetschka, G., Kostelecký, J. and Bezděk, A.: 2023b, Gravity aspects for Mars. Icarus, 406, 115729. DOI: 10.1016/j.icarus.2023.115729

Klokočník, J., Kostelecký, J., Bezděk, A. and Cílek, V.: 2023c, Hydrocarbons on Mars. Int. J. Astrobiol., 22, 6, 696–728. DOI: 10.1017/S1473550423000216

Kostelecký, J., Kalvoda, J., Klokočník, J. and Bezděk, A.: 2024, Mass density variations of landforms, active Orogeny and erosion in the Nepal Himalaya derived from the Earth Gravity Model EIGEN 6C4. In: The Nature of Geomorphological Hazards in the Nepal Himalaya. DOI: 10.1007/978-3-031-58421-3_6

Klokočník, J., Cílek, V., Kostelecký, J. and Bezděk, A.: 2025a, Popigai and Chicxulub craters: multiple impacts and their associated grabens. EGU Solid Earth, 16, 119–133. DOI: 10.5194/se-16-119-2025

Klokočník, J., Kostelecký, J. and Bezděk, A.: 2025b, Gravity strike angles from EIGEN6C4 to seek conditions favourable for hydrocarbon occurrences in the Arctic zone. Polar Sci., 43, 101157. DOI: 10.1016/j.polar.2024.101157

Klokočník, J., Kostelecký, J. and Bezděk, A.: 2025c, Groundwater at the Southern Pole of the Moon via the Gravity Strike Angles: IM-1 and Artemis. Planet. Space Sci., 256, 106037. DOI: 10.1016/j.pss.2025.106037

Konopliv, A.S., Park, R.S., Rivoldini, A., Baland, R.-M., Le Maistre, S. and Van Hoolst, T. et al.: 2020, Detection of the Chandler Wobble of Mars from orbiting spacecraft. Geophys. Res. Lett., 47, 21. DOI: 10.1029/2020GL090568

Lemoine, F.G., Goossens, S. et al.: 2014, A degree 900 lunar gravity model from GRAIL primary and extended mission data. Geophys. Res. Lett., 41, 3382–3389. DOI: 10.1002/2014GL060027

Masaitis, V.L.: 1998, Popigai crater: origin and distribution of diamond-bearing impactites. Meteorit. Planet. Sci., 33, 349–359.

Maus, S., Barckhausen, U., Berkenbosch, H., Bournas, N., Brozena, J., Childers, V., Dostaler, F., Fairhead, J.D., Finn, C., von Frese, R.R.B., Gaina, C., Golynsky, S., Kucks, R., Lühr H., Milligan, P., Müller, R.D., Olesen, O., Pilkington, M., Saltus, R., Schreckenberger, B., Thébault, E., Caratori Tontini, F.: 2009, EMAG2: A 2–arc min resolution Earth Magnetic Anomaly Grid compiled from satellite, airborne, and marine magnetic measurements. Geochem. Geophys. Geosyst., 10, 8. DOI: 10.1029/2009GC002471

Mizera, J. et al.: 2022, Parent crater for Australasian tektites beneath the sands of the Alashan Desert, Northwest China: Best candidate ever? In: L.C. Jurdy, D.M. Stein, C.A. Howard, K.A., Stein, S., eds., The Footsteps of Warren B. Hamilton: New Ideas in Earth Science. Geol. Soc. Am., 553, 25, 323–334. DOI: 10.1130/2021.2553(25)

Murphy, C.A.: 2007, Interpreting FTG gravity data using horizontal tensor components. EGM 2007 Int. Workshop on Innovation in EM, Grav. and Mag Methods: A new Perspective for Exploration, Capri, Italy, April 15-18.
DOI: 10.3997/2214-4609-pdb.166.A_OP_04

Murphy, C.A. and Brewster, J.: 2007, Target delineation using Full Tensor Gravity Gradiometry data. ASEG Extended Abstracts, 1, 1–3.
DOI: 10.1071/ASEG2007ab096

Murphy, C.A. and Dickinson, J.L.: 2009, Exploring exploration play models with FTG gravity data. 11th SAGA Biennial Technical Meeting and Exhibition., Swaziland, 16-18 Sept.
DOI: 10.3997/2214-4609-pdb.241.murphy_paper1

Özsöz, I. and Oruç, B.: 2023, Estimation of the hydrocarbon potentials of the Eastern Mediterranean basins from the Gravity Gradient Tensors. 21st Int. Petroleum and Natural Gas Congress and Exhibition (IPETGAS 2023), Sept., Ankara, Türkiye.

Pavlis, N.K., Holmes, S.A., Kenyon, S.C. and Factor, J.K.: 2008a, EGM2008: An overview of its development and evaluation. Conference on Gravity, Geoid and Earth Observation, Chania, Crete, June 23-27, 2008. National Geospatial-Intelligence Agency, USA.

Pavlis, N.K., Holmes, S.A., Kenyon, S.C. and Factor, J.K.: 2008, An Earth Gravitational Model to degree 2160: EGM2008. Geophys. Res. Abstr., 10, EGU2008-A-01891.

Pavlis, N.K., Holmes, S.A., Kenyon, S.C. and Factor, J.K.: 2012, The development and evaluation of the Earth Gravitational Model 2008 (EGM2008). J. Geophys. Res., 17, B04406. DOI: 10.1029/2011JB008916

Pajot, G., Diament, M., Lequentrec-Lalancette, M-F. and Tiberi, Ch.: 2004, Bayesian approach to invert GOCE Gravity Gradients. Proc. Second International GOCE User Workshop "GOCE, The Geoid & Oceanography", ESA-ESRIN, Frascati, Italy, 8-10 March (ESA SP-569).

Pedersen, B.D. and Rasmussen, T.M.: 1990, The gradient tensor of potential field anomalies: Some implications on data collection and data processing of maps. Geophysics, 55, 1558–1566. DOI: 10.1190/1.1442807

Pinter, N., Scott, A.C., Daulton, T.L., Podoll, A., Koeberl, C., Andrson, R.S. and Ishman, S.E.: 2011, The Younger Dryas impact hypothesis: a requiem. Earth Sci. Rev., 106, 247–264.
DOI: 10.1016/j.earscirev.2011.02.005

Pitoňák, M., Šprlák, M. and Tenzer, R.: 2017, Possibilities of inversion of satellite third-order gravitational tensor onto gravity anomalies: a case study for Central Europe. Geophys. J. Int., 209, 799–812.
DOI: 10.1093/gji/ggx041

Reimold, W.U., Koeberl, C., Gibson, R.L. and Dressler, B.O.: 2005, Economic mineral deposits in impact structures: a review. In: Koeberl, C., Henkel, H. (eds), Impact Tectonics. Springer, Berlin, Heidelberg, 479–552. DOI: 10.1007/3-540-27548-7_20

Saad, A.H.: 2006, Understanding gravity gradients- a tutorial. 25, 941–949. DOI: 10.1190/1.2335167

Schaetzl, R.J., Sauck, W.A., Heinrich, P.V., Colgan, P.M. and Holliday, V.T.: 2019, Commentary on Klokočník, J., Kostelecký, J. and Bezděk, A. 2019. The putative Saginaw impact structure, Michigan, Lake Huron, in the light of gravity aspects derived from recent EIGEN 6C4 gravity field model. J. Great Lakes Res., 45, 12–20. DOI: 10.1016/j.jglr.2019.07.006

Sebera, J., Wagner, C.A., Bezděk, A. and Klokočník, J.: 2013, Short guide to direct gravitational field modelling with Hotine's equations. J. Geod., 87, 223–238. DOI: 10.1007/s00190-012-0591-2

Smit, J. and Hertogen, J.: 1980, An extraterrestrial event at the Cretaceous–Tertiary boundary. Nature, 285, 198–200. DOI: 10.1038/285198a0

Sneh, A., Bartov, Y., Weissbrod, T.E. and Rosensaft, M.: 1998, Geological map of Israel. Ministry of National Infrastructures-Geological Survey of Israel.

Sturm, S., Wulf, G., Jung, D. and Kenkmann, T.: 2013, The Ries impact, a double-layer rampart crater on Earth. Geology, 41, 531–534. DOI: 10.1130/G33934.1

Visnevskyy, S. and Montanari, A.: 1999, Popigai impact structure (Arctic Siberia, Russia): Geology, petrology, geochemistry and geochronology of glass-bearing impactites. In: Large Meteorite Impacts and Planetary Evolution II., Geol. Soc. Am., Spec. Paper, 339, eds. B.O. Dressler B.O. and Sharpton, V.L., 19–60.

von Frese, R.R., Potts, L., Wells, S., Leftwich, T., Kim, H. et al.: 2009, GRACE gravity evidence for an impact basin in Wilkes Land, Antarctica. Geoch. Geophys. Geosyst., 10, 2, Q02014.
DOI: 10.1029/2008GC002149

von Frese, R.R., Kim, H.R., Leftwich, T.E., Kim, J.W. and Golynsky, A.V.: 2013, Satellite magnetic anomalies of the Antarctic Wilkes Land impact basin inferred from regional gravity and terrain data. Tectonophysics, 585, 185–195. DOI: 10.1016/j.tecto.2012.09.009

Wittke, J.H. and 27 others: 2013, Evidence for deposition of 10 million tonnes of impact spherules across four continents 12,800 y ago. Proc. the National Academy of Sciences of the United States of America, 110, E2088–E2097. DOI: 10.1073/pnas.1301760110

Wolbach, W.S. et al.: 2018, Extraordinary biomass-burning episode and impact winter triggered by the Younger Dryas cosmic impact ∼12,800 years ago, part 2: Lake, marine and terrestrial sediments. J. Geol., 126.
DOI: 10.1086/695704

Wood, J.R. and Harrison, W.B.: 1998, Advanced characterization of fractured reservoirs in carbonate rocks: the Michigan Basin. Rep. DE-AC26-98BC15100, Michigan TU, Houghton.

Zingerle, P., Pail, R., Gruber, T. and Oikonomidou, X.: 2019, The experimental gravity field model XGM2019e. ICGEM Potsdam. GFZ Data Services. DOI: 10.5880/ICGEM.2019.007